Student thesis series INES nr 359

Atmospheric Reactivity of Cyclic Ethers of Relevance to Biofuel Combustion

Emelie Linnéa Graham

2015
Department of
Physical Geography and Ecosystems Science
Lund University
Sölvegatan 12
S-223 62 Lund
Sweden

Emelie Linnéa Graham (2015).
Atmospheric reactivity of cyclic ethers of relevance to biofuel combustion

Master degree thesis, 30 credits in *Atmospheric Science & Biochemical Cycles*
Department of Physical Geography and Ecosystems Science, Lund University

Level: Master of Science (MSc)

Course duration: *January* 2015 until *June* 2015

Disclaimer

Atmospheric reactivity of cyclic ethers of relevance to biofuel combustion

---

Emelie Linnéa Graham

Master thesis, 30 credits, in
Atmospheric Science & Biochemical Cycles

Supervisor:

Elna Heimdal Nilsson
Combustion Physics, Lund University

Exam committee:

Thomas Holst
Physical Geography and Ecosystem Science, Lund University

Jimmy Heimdal
MAX IV Laboratory, Lund University

In loving memory of

Ulla Siv Graham
1931 – 2014

Abstract

Biofuels are considered to be an environmental friendly alternative to fossil fuels as they have the potential to reduce the global emissions of greenhouse gases. Studies have showed that an increased use of ethanol could alter the atmospheric chemical composition and enhance urban ozone concentrations resulting in higher human mortality rates. In recent years furanic compounds have been considered as second generation biofuels as they can be produced from non-food biomass. This project aims to improve the understanding of the impact of furanic biofuels in the atmosphere. Laboratory studies have been performed in smog chambers at Copenhagen Centre for Atmospheric Research and the University of Oslo, considering the reactions of furan, 2,3-dihydrofuran and 2,5-dihydrofuran with ozone and chlorine radicals. The furanic ozonolysis mechanism was further studied using computational methods.

The results of the relative rate studies show that furan reacts slower with both ozone and Cl than the two DHF do, while the reactions of 2,3-DHF with ozone and Cl is faster than the corresponding reactions of 2,5-DHF. When comparing the results with literature data it was found that furans will mainly decompose due to tropospheric reactions with OH. The furanic Cl reaction may become important, close to local chlorine sources, in highly polluted areas were elevated VOC concentrations result in increased competition for the tropospheric OH reaction. Furthermore it was found that 2,3-DHF react immediately with Cl_2, while furan and 2,5-DHF did not.

The results of the product study propose that furanic ozonolysis produces shorter oxygenated organic compounds, such as aldehydes and carboxylic acids. This study shows that furanic biofuels mainly decompose into atmospheric compounds associated with elevated tropospheric ozone levels and urban air pollution. Emission of these compounds to the atmosphere can therefore be expected to result in elevated levels of ground level ozone.

Keywords: Physical Geography and Ecosystem Science · 2nd Generation Biofuels Furans · Tropospheric Chemistry · Ozonolysis Atmospheric Kinetics IR Spectroscopy · Computational Chemistry

Svensk Sammanfattning

Biobränslen anses vara ett miljövänligt alternativ till fossila bränslen eftersom de har potential att minska de globala utsläppen av växthusgaser. Studier har visat att en ökad användning av etanol kan komma att påverka atmosfärens kemiska sammansättning och på så sätt bidra till förhöjda koncentrationer av marknära ozon, en luftförorening som är känd för att orsaka ökad dödlighet. Furaner kan framställas från bland annat mat- och skogsavfall och har därför introducerats som en andra generationens biobränslen. Detta projekt syftar till att förbättra förståelsen för hur furan-baserade biobränslen kan komma att påverka atmosfären. Laborationer har utförts i gaskammare vid Köpenhamns Universitet och Universitet i Oslo för att studera hur furan, 2,3-dihydrofuran och 2,5-dihydrofuran reagerar med ozon och fria klorradikaler. Vidare har den kemiska mekanismen för ozonolys av furaner studerats med hjälp av kemiska beräkningsmetoder.

De experimentella resultaten tyder på att furan reagerar långsammare med ozon och klor än vad de båda DHF gör, 2,3-DHF reagerar dessutom snabbare med ozon och klor än vad 2,5-DHF gör. Resultaten jämfördes med tidigare forskning och det kunde konstateras att furaner huvudsakligen reagerar med OH i troposfären. Däremot kan klorreaktioner komma att bli betydelsefulla nära lokala klorkällor, i kraftigt förorenade områden med ökad konkurrens om OH. Vidare visade studien att 2,3-DHF reagerar omedelbart med Cl_2, men att varken furan och 2,5-DHF gör det.

Produktstudien tyder på att ozonolys av furaner producerar korta syreinnehållande kolföreningar, så som aldehyder och karboxylsyror. Denna studie visar att furan-baserade biobränslen huvudsakligen bryts ner till kemiska föreningar som är associerade med luftföroreningar och förhöjda ozonhalter i troposfären. Utsläpp av olika furaner till atmosfären förväntas därför att resultera i förhöjda nivåer av marknära ozon.

Nyckelord: Naturgeografi och Ekosystemvetenskap · Andra Generationens Biobränslen Furaner · Troposfärskemi · Ozonolys Atmosfärskinetik · IR Spektroskopi Beräkningskemi

Acknowledgement

This project was performed at Combustion Physics, Lund University, as a part of a larger project dealing with the atmospheric reactivity of potential biofuels. The experimental studies were performed in laboratories at CCAR, University of Copenhagen and Department of Chemistry, University of Oslo.

First and foremost, I would like to thank my supervisor Elna Heimdal Nilsson for your guidance, advice and encouragement while working on this thesis and during previous projects. I value your input and appreciate your patience during my usually short and intense periods of writing. I am happy that you gave me the opportunity to participate in my first conference this year.

I would also like to thank Claus J. Nielsen for your creative ideas, quick response and generous help with the computations. I am grateful that you took the time to get the lab in shape for my final visit.

Thank you; Stina Ausmeel and Freja Østerstrøm for teaching me the procedure in the lab at CCAR, Matthew S. Johnson and Ole John Nielsen for your enthusiasm, and everyone I met at the departments in Oslo and Copenhagen.

I would like to express my gratitude to the foundations from which I have received scholarships this past year:

- Nordplus Higher Education programme.
- Nils Flensburgs travel scholarship fund.
- Foundation in memory of Fredrik Lindström.

Finally I wish to thank all my friends; this year would not have been the same without you guys! A special thanks to the Argiroudaki sisters for their warm hospitality while visiting Oslo. Last but not least, I am sending a warm thank you to my family for your endless support and encouragement to follow my own way.

Thank you all for believing in me when I had my doubts!

Table of Contents

Abbreviations

A	Absorbance
AO	Atomic Orbital
BVOC	Biogenic Volatile Organic Compound
c	Concentration
CCAR	Copenhagen Center for Atmospheric Research
CE	Cyclic Ether
CI	Criegee Intermediate
DFT	Density Functional Theory
DHF	Dihydrofuran
DME	Dimethyl Ether
DMF	Dimethylfuran
ε	Extinction coefficient
EtOH	Ethanol
FTIR	Fourrier Transform Infrared
GHG	Greenhouse Gases
HC	Hydrocarbon
HF	Harty Fock
HITRAN	High Resolution Transmission
$h\nu$	photon, with the frequency ν
I	Intensity at time t
I_0	Intensity at time 0
k_{2nd}	Second order rate constant
l	Path length
λ	Wavelength
LCA	Life Cycle Analysis
M	Atmospheric species in abundant
MALT	Multi-Atmospheric Layer Transmission
MO	Molecular Orbital
MS	Mass Spectrometry
MTHF	Methyltetrahydrofuran
NO_x	Nitrous Oxides
OVOC	Oxygenated VOCs
PAH	Polycyclic Aromatic Hydrocarbons
PAN	Peroxyacyl nitrates
PES	Potential Energy Surface
PM2.5	Particulate matter, diameter < 2.5 μm
PM10	Particulate matter, diameter < 10 μm
POP	Persistent Organic Pollutants

POZ	Primary Ozonide
ppb	Parts per billion
ppm	Parts per million
R_n	Hydrocarbon
$RC^{\bullet}O$	Acyl radical
RO_2	Peroxide
$RO^{\bullet}$	Alkoxy radical
$ROO^{\bullet}$	Peroxide radical
ROOH	Peroxide
T	Transmittance
τ	Atmospheric lifetime
THF	Tetrahydrofuran
TST	Transition State Theory
SCI	Stabilized Criegee Intermediate
SOA	Secondary Organic Aerosol
SOZ	Secondary Ozonide
QM	Quantum Mechanics
VOC	Volatile Organic Compound
ZPE	Zero point energy

Some Atmospheric Chemical Compounds

Name	Formula/Structure
Acetaldehyde	$CH_3C(O)H$
Acetyl Chloride	CH_3COCl
Acetylene	$HC{\equiv}CH$
Chlorine (radical)	$Cl^{\bullet}$
Chlorine (molecular)	Cl_2
Chlorine monoxide	ClO
Carbon dioxide	CO_2
Carbon monoxide	CO
Cyclohexane	c-C_6H_{12}
Cyclohexanone	c-$C_6H_{10}O$
Cycloheptene	c-C_7H_{12}
Dimethyl ether	CH_3OCH_3
Dinitrogen pentoxide	N_2O_5
Ethanol	CH_3CH_2OH
Excited oxygen atom	$O(^1D)$
Formaldehyde	$HC(O)H$
Formic acid	$HC(O)OH$
Hydrochloric acid	HCl
Hydrogen peroxide	H_2O_2
Hydroperoxyl radical	HO_2
Hydroxyl radical	OH
Hypochlorous acid	$HOCl$
Isobutylene	$CH_3C(CH_3){=}CH_2$
Methane	CH_4
Nitrate	NO_3
Nitric acid	HNO_3
Nitric oxide	NO
Nitrogen (molecular)	N_2
Nitrogen dioxide	NO_2
Nitrous oxide	N_2O
Nitryl chloride	$ClNO_2$
Oxygen (atomic)	$O(^3P)$
Oxygen (molecular)	O_2
Ozone	O_3
Propane	$CH_3CH_2CH_3$
Propene	$CH_3CH{=}CH_2$
Water	H_2O

1 Introduction

Over the last 100 years road transports have increased to become the largest emitter of greenhouse gases (GHG) in the transportation sector resulting in increased global warming (Uherek et al, 2010). Additionally, the pollution has local and regional effects since fossil fuels increase atmospheric nitrous oxides (NO_x), causing photochemical smog consisting of ozone and particulate matter, see Figure 1.1. Ethanol was introduced as a clean and renewable, alternative energy source with the aim to decrease the global environmental effects of road transportation. In recent years it has been suggested that, since ethanol has other reaction by-products compared to fossil fuel combustion, an increased use of ethanol will alter the atmospheric chemical composition (Andersen, 2012). This in such a way that it may enhance future urban ozone concentrations resulting in higher human mortality rates (Jacobson, 2007). Furthermore, recent studies suggest that the climate change could alter the tropospheric chemistry in such way that human mortality rates would increase due to the associated air pollution (Fang et al., 2013).

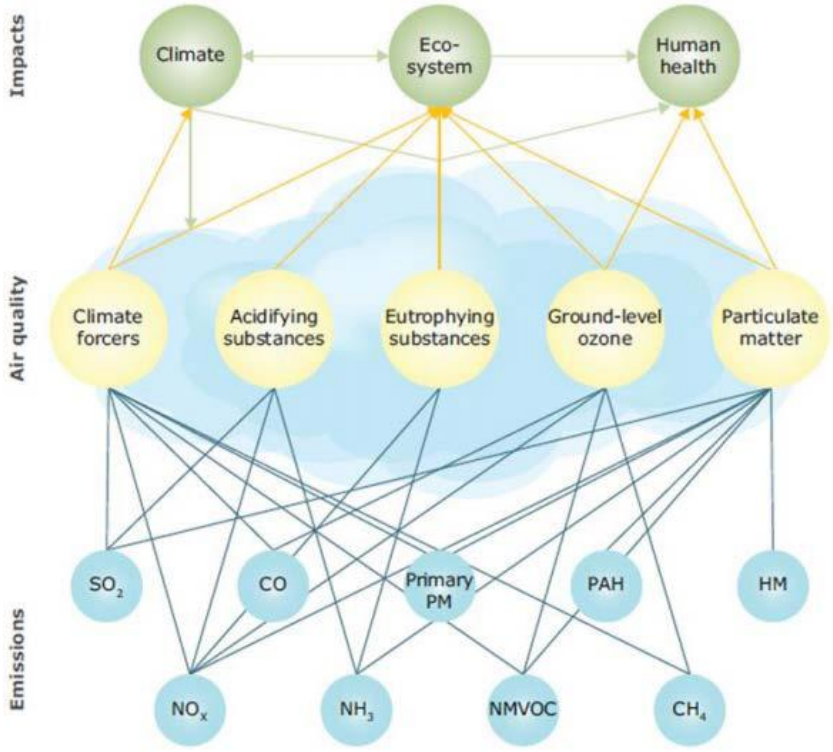

Figure 1.1 Emissions of atmospheric pollutants and their related impacts on the climate, environment and human health. The pollutants, presented from the left to the right, are: sulphur dioxide (SO_2), carbon monoxide (CO), primary particulate matter (PM), polycyclic aromatic hydrocarbons (PAH), heavy metals (HM), nitrogen oxides (NO_x),ammonia (NH_3), non-methane volatile organic compounds (NMVOC) and methane (CH_4) (Souce: EEA, 2014).

Since the first generation biofuels (including ethanol) is being produced from food crops, alternative compounds that do not compete with the food market have been suggested as a second generation biofuels. Among them are furanic fuels consisting of five membered cyclic ethers (CE) that can be produced from crop residues and forest waste (Sy Tran et al, 2012). Furans are predicted to have a short atmospheric lifetimes, i.e. their atmospheric decomposition will mainly affect regional air quality. Today's high demand for new fuels and energy sources requires an understanding of the processes on the molecular level so that it can be improved on a larger scale. In addition, knowledge about the combustion process is important in order to estimate the production of new pollutants. A life cycle analysis, describing the furanic fuel emissions from production, via leakages and the final emissions through non complete combustion, can determine at what magnitude furanic fuel may affect the atmospheric chemical composition (Scovronick & Wilkinson, 2014). Trying to describe the effects caused by an introduction of new pollutants is a complex process, illustrated in Figure 1.1, as it may affect the atmospheric environment in several ways, e.g. through aerosol formation, smog and the greenhouse effect.

This project focuses on some of the chemical reactions that will take place once the furanic fuel finally enters the atmosphere. The aim is to determine the atmospheric lifetimes and products from the reaction of furan, 2,3-dihydrofuran (2,3-DHF) and 2,5-dihydrofuran (2,5-DHF), see Figure 1.2 for the their chemical structures, with ozone (O_3) and chlorine radicals (Cl). Recent studies suggest DHF to be reaction products of furanic combustion (Kasper et al., 2010). Cl is predicted to affect the air quality close to local sources through chemical reactions similar to the reactions with the hydroxyl radical in the troposphere (Andersen et al., 2012) Detailed information about atmospheric chemical kinetic and decomposition mechanisms may be implemented in atmospheric chemical models describing the lifetimes and distribution of potential pollutants. The information is important as part of the scientific understanding required when evaluating the environmental impact of these potential biofuels.

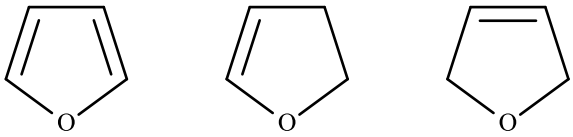

a) b) c)

Figure 1.2 The chemical structure of
a) Furan b) 2,3-Dihydrofuran c) 2,5-Dihydrofuran

1.1 Aim

This project aims to improve the understanding of the atmospheric impact related to an introduction of furanic fuels to the biofuel market. This is done by:

- Experimental kinetic studies, determining the reaction rate constants and related atmospheric lifetimes for the reactions of furan, 2,3-DHF and 2,5-DHF with ozone and free chlorine radicals.
- Theoretical mechanistic studies, focusing on the furanic ozonolysis.

Questions to be answered during the project are:

1) How does the rate of saturation affect the atmospheric furanic reactivity towards ozone and free chlorine radicals?
2) How does the oxygen position in relation to the double bond affect the atmospheric DHF reactivity?
3) How does the atmospheric furanic reactivity towards Cl differ from its reactivity towards OH?
4) What are the furanic atmospheric lifetimes in urban and rural environments respectively?
5) Which pollutants are related to the atmospheric furanic ozonolysis?

1.2 Outline

The report is divided into three separate sections describing the background, the experimental and theoretical methods and the results. Part I consists of two chapters dealing with urban air pollution and an overview of the atmospheric chemistry related to biofuel combustion. A more detailed description of the relevant atmospheric chemical reactions is presented in Appendix A. Part II describes the methodology of the laboratory studies and the following data analysis together with a description of the mechanistic and product study. Part III presents, discusses and concludes the results of the project.

PART I – BACKGROUND

Part I of the report describes the scientific background of the project. Chapter 2 presents the sources of urban air pollution and Chapter 3 describe the atmospheric properties of biofuels. Numbers within parenthesis refer to the atmospheric chemical reactions described in more detail in Appendix A.

2 Urban Air Pollution

"…a cloud of sea-coal, as if there be a resemblance of hell upon Earth,
it is in this volcano in a foggy day: this pestilent smoak, which corrodes the yron,
and spoils all the moveables leaving soot on all things that it light and so fatally siezing
on the lungs of the inhabitants, that cough and consumption spare no man…"

This is how London air quality was described by John Evelyn in his book *Fumifugium: or, The Inconveniencie of the Aer and Smoak of London Dissipated*, published in 1661. This kind of pollution associated with coal combustion, referred to as classical smog, came to be a concern in most European industrial centres during the nineteenth century. The most well-known event took place in London 1952; heavy fog covered the city and its surroundings for several weeks causing more than 4000 deaths as a result of respiratory problems (vanLoon & Duffy, 2011). Just a few years later, in 1955, down town Los Angles suffered a severe smog event, measuring ozone mixing ratio at 680 ppb (which still remains the highest level ever recorded). Today it is well known that the properties of the Los Angeles smog differ from classical smog and will hereafter be referred to as photochemical smog (Seinfeld & Pandis, 2006). The elevated ozone levels are to a large extent generated by the photochemistry of products related to fossil fuel combustion, mainly emitted by vehicles. Rigorous emission regulations have been able to reduce urban classical smog since the 1950's, while photochemical smog is still an increasing problem due to the heavy traffic loads in the city centres. Today tropospheric ozone concentrations generally fluctuate between 20 – 60 ppb and can exceed 100 ppb in urban areas, while levels above 200 ppb are considered severe air pollution (Seinfeld & Pandis, 2006). Many of the largest metropolises in the world suffer from major health problem as a result of urban photochemical smog.

This chapter will have a look into the properties of urban air pollution and how it fluctuates during the day. The first section describes the well-established properties of tropospheric ozone followed by a section concerning chlorine as a newly proposed component affecting the urban air quality.

2.1 Ozone

Atmospheric scientist distinguishes between the "good" stratospheric ozone (with maximum concentrations around 25 km altitude), which protects all biological life forms from the harmful intense short wave solar radiation, and the "toxic" tropospheric ground level ozone (Seinfeld & Pandis, 2006). The latter is being produced in a set of chemical reactions, summarized in Figure 2.3 and described further in section 2.1.1. Tropospheric ozone production is initiated by the photochemical destruction of NO_2, commonly associated with fossil fuel combustion and biomass burning. Photolysis of NO_2 results in NO and together they form the atmospheric NO_x family, mainly emitted in the form of NO which is rapidly oxidized into NO_2 (A2.3, A3.3, A5.5).

Due to its photochemical origin, i.e. sunlight is required, tropospheric ozone levels display a characteristic diurnal profile, which is evident from Figure 2.1. A minimum is found in the morning, just before the morning traffic begins and urban NO_x concentrations increase drastically. Ozone levels starts to grow as a result of the sunrise, combined with the NO_x emission, and reaches its maximum during the afternoon. Urban ozone levels usually peaks between 15.00 - 17.00 p.m. but can vary significantly depending on the meteorological conditions, season and latitude (Klumpp et al., 2006).

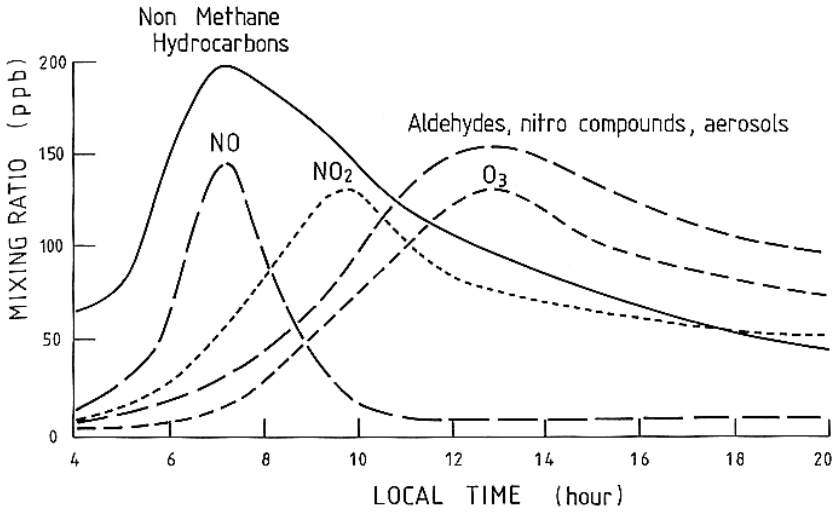

Figure 2.1 Daily evolutions of atmospheric trace gases under polluted conditions in urban areas. (Source: Harrison, 1990)

As the sun sets, the photochemistry slows down and finally stops during the night. NO are no longer being produced, hence neither is ozone, while NO_2 take part of the night time ozone destruction (A6.1) and finally deposit as nitric acid, HNO_3 (A2.6 & A6.4 represent the mayor removal of atmospheric NO_x). The stable nocturnal boundary layer prohibit turbulent mixing and ozone levels drops, reaching its minimum just before sun rise when a new diurnal cycle begin. With an exception found in coastal areas, see Edinburgh in Figure 2.2, were the night breeze counteracts the nocturnal

inversion. The night time sea breeze circulation may entrain ozone-rich air masses resulting in lower ozone depletion (Klumpp et al., 2006).

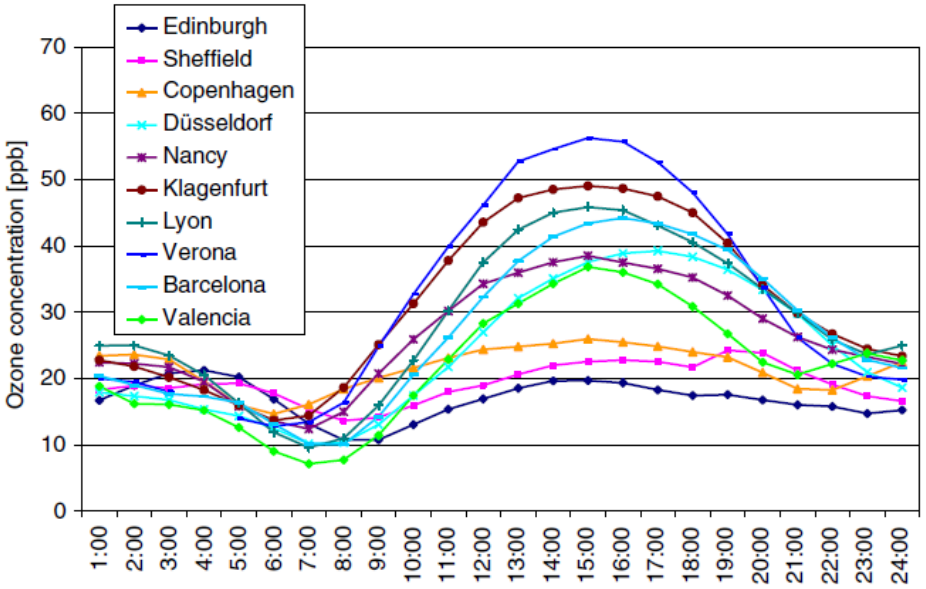

Figure 2.2 Case study of the mean diurnal ozone levels in European sites during April to September in 2001, presenting the ozone concentration (ppb) versus the local time (hours). Ozone variability increases along a north to south gradient. (Source: Klumpp et al. 2006)

In 2006, Klumpp et al. presented a case study of the European urban ozone levels during the summer of 2001. This year can be considered to be a 'normal' year regarding both meteorological conditions and ozone levels, which were lower than in the hot summer of 2003, while higher than in the cold and moist summer of 2002. With one exception in Scandinavia, that experienced unusually low ozone levels.

Figure 2.2 presents the mean diurnal ozone levels in a set of European cities during April to September, 2001. Suburban areas experience lower ozone variability due to fewer pollutants, in these areas most of the ozone was produced in more polluted areas and then transported. Here the lifetime of ozone can be significantly higher since the lower NO_x levels results in reduced ozone quenching, which may cause suburban ozone levels to be almost three times as high as in the closest city during the night time.

As a result of the radiation dependency, ozone variability increases along a north to south gradient. Simply explained, ozone production increases to the south as the short wave radiation, initiating the photochemistry, becomes more intense. Additionally, ozone production, hence variability is more pronounced in mountainous areas, such as the Alps. In cities located in valleys the pollutants may be trapped during longer periods affecting the local ozone levels for a longer time. See for example Klagenfurt, Austria, showing the second largest variability in Figure 2.2, which is larger than the two more southern locations, Barcelona and Valencia, Spain.

2.1.1 The Ozone Isopleth

In the prior section ozone production is discussed from an isolated NO_x perspective, this is not the case in the more complex atmosphere, especially not in a polluted troposphere. In the isolated NO_x cycle, see Figure A2, nitrous oxide is being oxidized by ozone resulting in a balance between produced and consumed ozone. While in the atmosphere, the key to tropospheric ozone formation is the hydroxyl radical (OH). It is often referred to as the detergent of the atmosphere as it is highly reactive towards volatile organic carbons (VOC). The OH reaction with VOC produces the hydroperoxyl radical (HO_2) (A5.1-A5.6), which in turn oxidizes NO into NO_2 (A3.3) and OH is regenerated, hence there is a net production of ozone, as described in Figure 2.3.

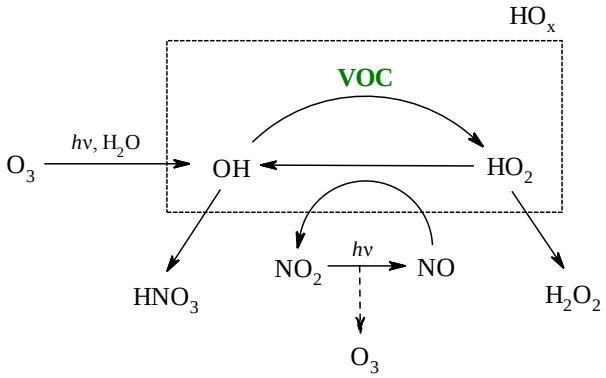

Figure 2.3 Tropospheric ozone production under polluted conditions in urban areas.
(Derived from the tropospheric chemistry presented in Seinfeld & Pandis, 2006)

OH is the main tropospheric oxidant and there is a constant competition for its reaction. At high NO_x concentration ozone production becomes terminated via (A2.6) producing nitric acid (HNO_3) which is mainly removed from the atmosphere through dry deposition. These conditions are referred to VOC-limited as the ozone production is linearly dependent on the VOC concentrations. Under so called NO_x limited conditions the OH production slows down as (A3.3) occurs less frequent. As a result, NO_x concentrations determine if an area is a source or a sink of ozone (Seinfeld & Pandis, 2006). The maximum ozone yield can be described using an ozone isopleth diagram which is a contour plot as a function of the initial VOC and NO_x concentrations. Figure 2.4 is an example of an ozone isopleth diagram describing the maximum achieved ozone concentrations (see the contour lines) integrated over a 10 h time period using a generalized VOC/NO_x mechanism.

In the case of NO_x limited conditions, see for example 4 ppb in Figure 2.4, VOC concentrations could be substantially increased, from 100 to 200 ppb, only resulting in a slightly increased ozone concentration, from 150 to 180 ppb. On the contrary, for higher VOC concentration around 300 ppb a small increase in NO_x, from 4 to 10 ppb, results in a major increase in ozone concentrations, from 180 to 240 ppb.

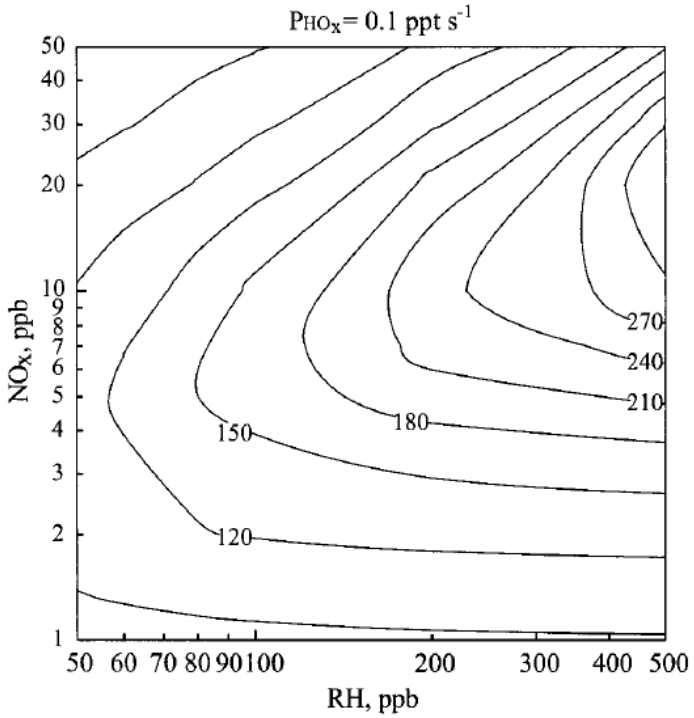

Figure 2.4 Example of an isopleth diagram describing the maximum tropospheric ozone concentrations (ppb) integrated over a ten hour period as a function of the initial VOC (RH) and NO_x concentrations. (Source: Seinfeld & Pandis, 2006)

2.2 Chlorine

The chlorine radical (Cl) is known to affect the atmospheric chemistry in coastal regions as a result of its relatively high concentrations. In recent years it has been suggested that Cl may also affect locally around anthropogenic sources like factories were chlorinated solvents are used. Cl is released through photo dissociation of these compounds, mainly Cl_2 and nitryl chloride ($ClNO_2$) (A4.1), resulting in concentration ranging from $10^2 – 10^5$ molecules cm^{-1} (Young et al, 2014).

Cl generally oxidizes VOC in the same manner as OH do, via hydrogen abstraction (A4.5) (Andersen et al., 2012). But the chlorine radical differs from OH in two aspects (Young et al. 2014):

1. Cl react more rapidly with VOC, with the reaction rate constant usually being over one magnitude larger than for the corresponding OH reaction. Cl is especially reactive towards some alkanes which are known to rarely react with OH. The high Cl reaction rate results in a shorter atmospheric lifetime and smaller abundance, in polluted areas with high Cl emissions.

2. The largest daily loss of OH, up to 30 %, is due to termination through production of nitric acid, HNO_3 (A2.6) preventing it from oxidizing VOC. Cl, on the other hand, is less reactive towards NO_2 and more effective at initiating chain reactions. Through VOC oxidation Cl is able to increase tropospheric OH concentrations, see Figure 2.1, and the tropospheric oxidative cycle becomes even more effective in producing ground level ozone (Chang & Allen, 2006). Finally Cl terminate through a set of reactions forming hypochlorous acid (HOCl) (A3.5, A4.6) and chlorine monoxide (ClO) (A4.2).

In the morning photochemistry kicks in due to the increased solar radiation and $ClNO_2$ is being photo dissociated into free chlorine radicals resulting in a sharp Cl peak between 07.00 – 11.00 a.m., see Figure 2.6. Hence, Cl has the largest effect on urban air quality during morning traffic, the same time as the majority of other pollutants are being emitted. During this time of the day Cl represents more than half of all primary radicals (down town Los Angeles) and may cause as much as a 70 ppb increase in local ozone concentrations (measuring 1 h mean value) (Chang & Allen, 2006). The effect of Cl on ozone concentrations are reduced to about 10 ppb during the rest of the day. In the evening photochemistry slows down and the majority of the free chlorine radicals starts to react with NO_2 reforming nitryl chloride, $ClNO_2$ (A4.4b).

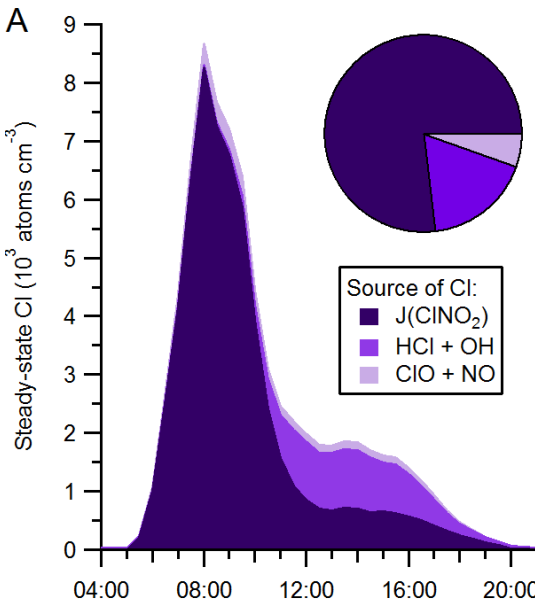

Figure 2.5 Diurnal Cl concentrations, estimated from measurement of different photochemically induced precursors, revealing a sharp peak during the morning hours. (Source: Young et al. 2014)

3 Biofuels

> "Biofuel is a chemically very heterogeneous and variable term...
>
> …It may thus be wiser to judge a biofuel beyond its economic viability or technical ease of adaptation to the present combustion environment."
>
> Kohse-Höninghaus et al. (2010)

Biofuels are considered to be an environmental friendly alternative to fossil fuels as they have the potential to reduce the global emissions of GHG. In fact, some of the first engines were actually designed to run on vegetable oil and ethanol-gasoline blends, but were outcompeted by the low oil prices during Second World War (Andersen, 2012). During the seventies oil crises ethanol (EtOH) was once again considered as an alternative fuel and is today, together with biodiesel, a commonly used biofuel. This chapter presents a short description of some common biofuels and their related impact on the urban air composition

3.1 Environmental Impacts

Biofuels can be divided in three generations considering the origin of the feedstock. The first generation, which is commercially available today, is competing with the food market as it is being produced from feedstock such as sugar- and oil crops. First generation biofuels comprises of alcohols and biodiesel, fatty acids produced from vegetable oils, both may be used as additives or substitutes to traditional fuels (Andersen, 2012). Biogas is an additional, more niched, first generation biofuel produced under anaerobic treatment of bio waste (Naik et al., 2010). In contrast to its procedures, the second generation biofuels are produced from non-edible plants parts, including alcohols and biodiesel together with new compounds such as cyclic ethers. Finally, the third generation is mainly biodiesel being produced from algae (Scovronick & Wilkinson, 2014). The following text will focus on the environmental effects related to the first generation biofuel production and usage.

Fossil fuel based combustion generally produces polyaromantic hydrocarbon (PAH) and soot precursors. EtOH blends are known to decrease these emissions, while increasing the production of carbonyls, such as acetone and aldehydes. Hence, the combustions chemistry of biofuels, which are oxygenated hydrocarbons, differs from traditional fossil fuels, i.e. hydrocarbons, in the sense that the C–O bond alters the electronic structure of the molecule affecting the strength of the C–H bonds (Kohse-Höinghaus et al., 2010). Atmospheric emissions of aldehydes results in enhanced tropospheric levels of ozone and peroxyacyl nitrates (PAN) (A7-A11), a compound related to photochemical smog causing respiratory problems. The combustion chemistry of dimethyl ether (DME), the isomer of EtOH, differs slightly as a result of its chemical structure. DME blends tend to

produce higher mole fractions of formaldehyde (HC(O)H) than EtOH-blends, for which the mole fraction of acetaldehyde (CH_3CHO) are higher (Kohse-Höinghaus et al., 2010). This can be explained by the absence of a C–C bond in DME, demonstrating the importance of understanding the difference in the chemistry of isomers.

Jacobson (2008) showed that the amount of unburned EtOH released into the atmosphere actually results in higher concentrations of acetaldehyde than the total combustion emissions. Additional atmospheric effects arise from emissions while storing and distributing the fuel. Biofuels are generally compounds with shorter carbon chains than gasoline and diesel, meaning that they tend to be more volatile (Andersen, 2012). As a result larger fractions of the biofuel may reach the atmosphere through unwanted emissions affecting the surrounding air quality. Traditional fuels are made more volatile when blended with an additive, e.g. gasoline with EtOH, resulting in higher evaporation rates and increased ground level ozone. Moreover, there is a risk that biofuel additives could prolong the persistence of petroleum related toxins in the nature as a result of increasing their solubility (Scovronick & Wilkinson, 2014).

Primary soot particles (PM2.5) are an indirect air pollution related to first generation biofuels as they are emitted from biomass burning during the production phase. Pollution of waterbodies and soils related to first generation biofuels are mainly caused by the usage of fertilizers and pesticide during the production phase. Nitrous based fertilizers do not only contribute to eutrophication, but emissions of N_2O have severe effect on earths radiation budget as it is a strong GHG with a global warming potential almost 300 times higher than CO_2.

There are still additional uncertain health- and environmental related effects to the biofuel production. An industrial expansion could contribute to water scarcity, as the production of biological matter require orders of magnitude more water than the traditional petroleum industry. Finally, the land-use change related to the production of biofuels would result in severe effects on the ecosystems and the climate (Scovronick & Wilkinson, 2014).

3.2 Cyclic Ethers

Plant biomass represents the most abundant biological energy source on earth, which in its pure form can be burnt to produce heat and electricity, while the production of food crops only utilises approximately 1.25 % of earth's biomass (Naik et al., 2010). Second generation biofuels is based on lignocellulosic materials obtained from crop residues and forest waste (Sy Tran et al., 2010). Figure 3.2 illustrates how biomass is being fragmented into smaller the components, either cellulose or hemicellulose followed by several reaction steps, in the production of furanic fuels, i.e. cyclic ethers such as furan, 2-metyltetrahydrofuran (2-MTHF) and 2,5-dimethylfuran (2,5-DMF) (Voll & Marquardt, 2012).

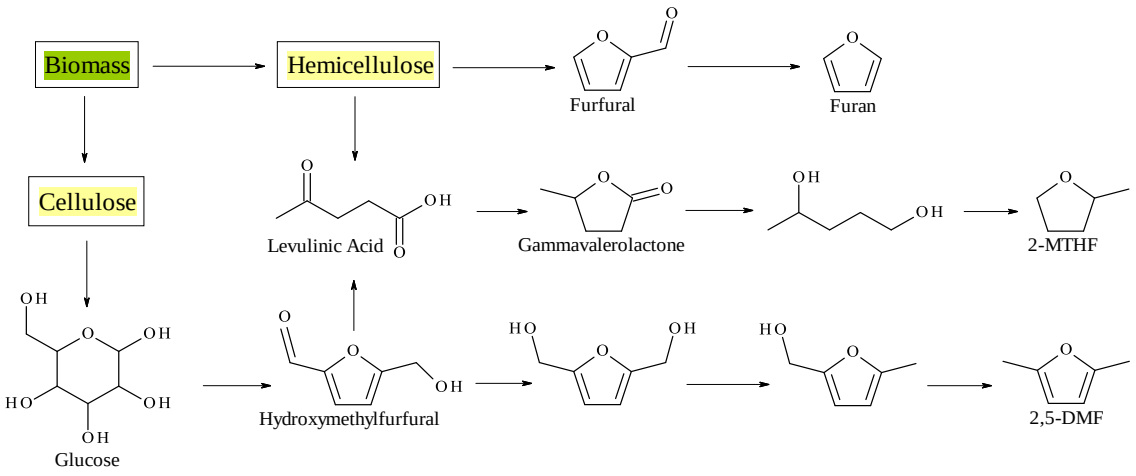

Figure 3.2 Reaction network describing the processing of biomass into becoming furanic fuels, such as furan, 2-metyltetrahydrofuran and 2,5-dimethylfuran. (Derived from Voll & Marquardt, 2012)

Furans are known to be produced via the oxidation of common atmospheric compounds such as isoprene and aromatics (Cabañas et al., 2005). Compared to EtOH, furanic fuels are less volatile and have higher energy density, close to gasoline; hence their combustion characteristics are similar to gasoline (Sy Tran et al., 2010). Furanic fuel combustion produces large amounts of organic compounds such as acetylene (C_2H_2), alkenes, aldehydes, cyclic compounds and aromatics, which are a commonly known to be soot precursor (Sirignano et al., 2010, Kasper et al., 2010). However, furanic fuels are based on oxygenated hydrocarbons and the resulting combustion emission should therefore differ from traditional hydrocarbon based fuels.

3.2.1 Furan & DHF

In this project the atmospheric reaction of three furanic compounds have been studied, namely furan, 2,3-DHF and 2,5-DHF, see Figure 1.2 for their chemical structure. Furan is both considered as a fuel and is part of the structure of other furanic fuels, while DHF have been detected as decomposition products during the combustion of tetrahydrofuran (THF) (Kasper et al, 2010). Additionally, all three compounds are interesting as they are potential atmospheric reaction products from similar furanic compounds or other common tropospheric VOC, such as isoprene (Cabañas et al., 2005).

The reaction rate constants for the atmospheric reaction of all three furans with ozone, Cl and OH have been determined before; see previous data in Table 3.1. However, there is very little information about the atmospheric fate of these compounds. Due to the larger molecular structures, compared to EtOH, furanic combustion is expected to result in broad spectra of potential combustion- and atmospheric reaction products.

Table 3.1 Summary of the previously determined furanic reaction rate constants, k (cm^3 $molec^{-1}$ s^{-1}), with ozone, Cl and OH.

	$k_{O_3} \cdot 10^{18}$	$k_{Cl} \cdot 10^{10}$	$k_{OH} \cdot 10^{11}$
Furan	2.42 ± 0.28 [1]	2.0 ± 0.2 [2]	4.01 ± 0.30 [3]
2,3-DHF	4432 ± 790 [4]	4.52 ± 0.99 [5]	6.45 ± 1.69 [4]
2,5-DHF	16.5 ± 3.1 [4]	4.48 ± 0.59 [5]	11.95 ± 2.79 [4]

[1] Graham, 2013.
[2] Cabañas et al., 2013.
[3] Atkinson et al., 1983.
[4] Alwe et al., 2014.
[5] Alwe et al., 2013.

PART II – METHOD

Part II presents the methods applied in the project. Figure 4.1 illustrates the different parts of the work process in order to determine an atmospheric decomposition mechanism of a specific compound. Part II is divided in two separate chapters describing the experimental- and theoretical methodology, see Chapter 4 and 5 respectively.

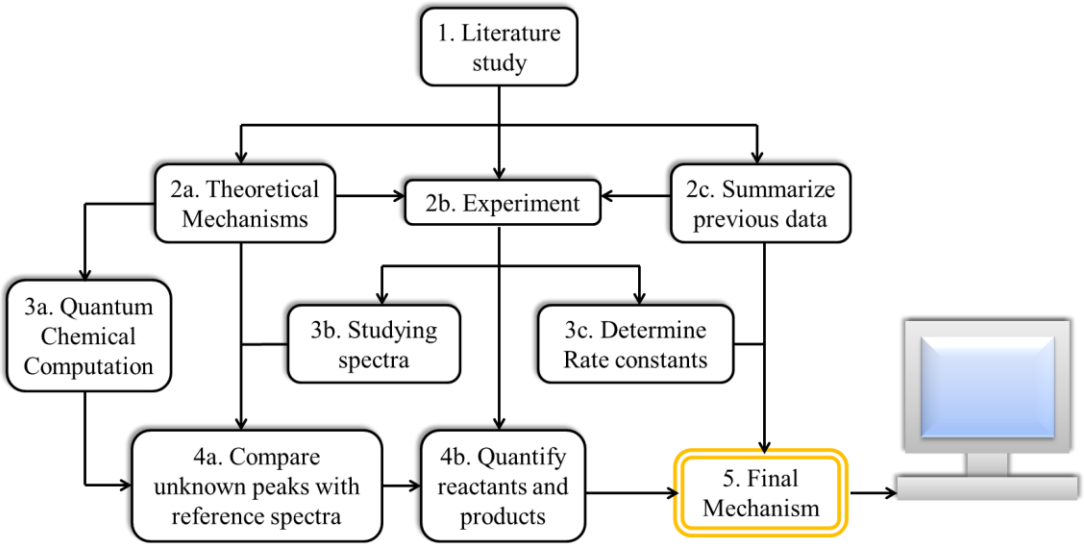

Figure 4.1 Illustration of the work process during the project.

4 Laboratory Study

When studying atmospheric chemical reactions it is desirable to simulate atmospheric conditions in the laboratory (Nilsson et al, 2009a). Low pressure, hence low concentration, prevents secondary chemistry to take place in the sample while at the same time lowering the sensitivity of the detector. In this project smog chambers connected to FTIR spectrometers have been used. The chambers are equipped with a multipass optical system which increases the optical path length through the sample and therefore enhances the sensitivity of the detector. This chapter begins with an introduction to some necessary chemical kinetics followed by a brief description of the optical techniques of FTIR spectrometry. Finally the experimental setup and procedures in the two laboratories (CCAR, University of Copenhagen and Department of Chemistry, University of Oslo) are presented separately (Figure 4.1:2b). Previously recorded spectra were used for the mechanistic studies of the atmospheric furanic reactions. The methodology for the product analysis is presented in the separate chapter, 5 Mechanistic Study.

4.1 Chemical Kinetics

There are three types of chemical reactions relevant to atmospheric chemistry:

$$\begin{array}{lll} \text{First}-\text{order} & \text{A} \rightarrow \text{B} + \text{C} & (\text{unimolecular}) \\ \text{Second}-\text{order} & \text{A} + \text{B} \rightarrow \text{C} + \text{D} & (\text{bimolecular}) \\ \text{Third}-\text{order} & \text{A} + \text{B} + \overset{\text{M}}{\rightarrow} \text{AB} & (\text{termolecular}) \end{array}$$

In the atmosphere the first order reaction is mainly represented by photo dissociation of compound A into compounds B and C. The third-order reaction represents the reaction of the two molecules A and B forming an excited intermediate $AB^{\ddagger}$ which de-excites through collision with a stable molecule, M, usually in excess in the atmosphere (e.g. N_2 and O_2).

This project focuses on the atmospheric second-order reaction of three unsaturated cyclic ethers (CE) with ozone and Cl, and the rate of this bimolecular reaction is as follows:

$$\frac{d[\text{CE}]}{dt} = -k_{2\text{nd}} \cdot [\text{CE}] \cdot [\text{R}] \qquad \text{Eq. 4.1}$$

were [CE] and [R] are the concentrations of the reactants, i.e. furans and ozone or Cl respectively, and $k_{2\text{nd}}$ is the second-order reaction rate constant, describing the speed of the reaction (Seinfeld & Pandis, 2006). $k_{2\text{nd}}$ may be determined using the absolute- or relative rate method, depending on the chemistry and experimental setup.

Once the reaction rate constant is known it is possible to determine the atmospheric lifetime, τ_{CE}, of the compound, CE, in relation to the specific reactant, R:

$$\tau_{\text{CE}} = \frac{1}{k_{2\text{nd}}[\text{R}]} \qquad \text{Eq. 4.2}$$

4.1.1 Absolute Rate Method

With one of the reactants, R, in abundance, compared to the other one, its concentration can be considered being constant throughout the experiment. According to the absolute rate method Eq. 4.1 can be rewritten as:

$$\frac{d[\text{CE}]}{dt} = -k_{\text{abs}} \cdot [\text{CE}]$$

were k_{abs} is the reaction rate constant. Through integration and rearrangement the linear expression is obtained:

$$\ln\left(\frac{[\text{CE}]_t}{[\text{CE}]_0}\right) = -k_{\text{abs}} \cdot t \qquad \text{Eq. 4.3}$$

were the $[\text{CE}]_t$ and $[\text{CE}]_0$ are the concentrations of CE at the time 0 and *t*, respectively.

k([R]) is obtained via the linear regression of the logarithmic decay of [CE] versus time, see Figure 4.2a. The final reaction rate coefficient, k_{abs}, independent of [R], corresponds to the slope of the linear fit of all k([R]) as a function of the varied concentration of R, see Figure 4.2b. The absolute rate method is only valid if loss of CE is limited to the reaction with R, and [R] is in excess compared to [CE].

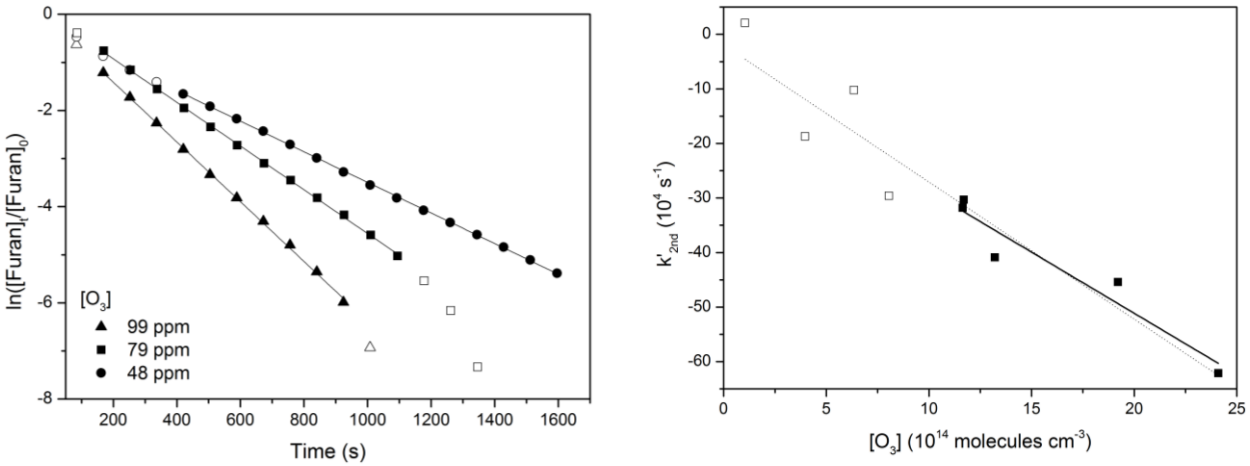

a) b)

Figure 4.2 Example of results using the absolute rate method, were the final absolute rate constant correspond to the slope of the solid line in b). (Graham, 2013)

4.1.2 Relative Rate Method

If the initial concentration of one of the reactants is unknown, e.g. during photo initiated experiments, a reference compound with the known rate constant, k_{ref}, may be included. The relative rate methods assume simultaneous reactions of CE and the reference compound, ref, with R and results in a linear equation system with two unknown variables, k_{rel} and [R]:

$$\begin{cases} \frac{d[\mathrm{CE}]}{dt} = -k_{\mathrm{rel}} \cdot [\mathrm{R}] \cdot [\mathrm{CE}] \\ \frac{d[\mathrm{ref}]}{dt} = -k_{\mathrm{ref}} \cdot [\mathrm{R}] \cdot [\mathrm{ref}] \end{cases}$$

Through integration, rearrangement and division of the two equations the unknown reactant concentration, [R], is cancelled out and the linear expression is obtained:

$$\ln\left(\frac{[\mathrm{CE}]_0}{[\mathrm{CE}]_t}\right) = \frac{k_{\mathrm{rel}}}{k_{\mathrm{ref}}} \ln\left(\frac{[\mathrm{ref}]_0}{[\mathrm{ref}]_t}\right) \qquad \text{Eq. 4.4}$$

k_{rel} is obtained from the slope of the linear regression when plotting the logarithm of the furan decay versus the logarithm of the reference compound decay (D'Anna et al., 2005). The relative rate method is only valid if the losses of CE and the reference compound are limited to the reactions with R.

4.2 Optical Techniques

In the same way as the GHG absorb light of specific wavelengths, resulting in the characteristic atmospheric radiation window; different molecular functional groups are associated with light absorption in different wavelength regions. In this sense, a photoreactor simulates the atmosphere and the detected spectra can be related to the samples chemical composition and concentrations.

Beer-Lamberts law states that the detected intensity of a light beam passing through a sample with the concentration, *c*, and path length, *l*, can be expressed as:

$$I(\lambda) = I_0(\lambda) \cdot 10^{-\varepsilon(\lambda)cl} \qquad \text{Eq. 4.5}$$

were I_0 is the intensity of the incident light and ε is the wavelength dependent extinction coefficient (Atkins & de Paula, 2010). As the detected intensity is the transmitted light, *T*, it is related to the absorption, *A*, of the sample:

$$A = -\varepsilon(\lambda)cl = -\log\frac{I}{I_0} = -\log T \qquad \text{Eq. 4.6}$$

A samples extinction coefficient depends on the molecular vibrational frequency and is therefore related to the atom masses and the force constant of the molecular bonds (Engel, 2013). As a result different functional groups exhibit characteristic infrared absorption bands, which will be discussed more in detail in Chapter 5.2.1, hence the combination of different functional group makes each molecular absorption spectrum unique.

4.2.1 FTIR Spectroscopy

Fourier Transform Infrared (FTIR) spectroscopy is a useful tool for recording wide range absorption spectra in a short time. Compared to a traditional absorption spectrometer that records the absorption for each wavelength at a time, it combines a broadband blackbody radiation source and a Michelson interferometer (Engel, 2013). The interferometer contains a beam splitter dividing the light beam in two perpendicular beams which are recombined through reflection by two mirrors. As one of the mirrors is being movable, the detector records a time resolved interference pattern called an interferogram. Finally, the infrared absorption spectrum is obtained through Fourier transformation of the interferogram.

4.3 Chlorine Kinetic Experiment

Chlorine experiments were carried out in the photoreactor at CCAR, Department of Chemistry, University of Copenhagen, following the relative rate method.

4.3.1 Experimental Setup

The photochemical reactor is constructed of a 100 L quartz cylinder, transparent at wavelengths > 190 nm, sealed with electropolished stainless steel end flanges (Nilsson et al, 2009a). It is connected to a Vacuum FTIR interferometer (Bruker IFS 66v/s) and the IR beam is reflected back and forth in the chamber via a White-type multiple reflection system, see Figure 4.3. The optical path length was calibrated to be 50.31 m, but was reduced to 42 m (May 6th 2015) due to problems with the experimental setup. The transmitted beam is detected using a narrow band Mercury Cadmium Tellurium (MCT) detector with the resolution set to be 0.25 cm^{-1} (determined by the spectrometer). The chamber is placed in an insulated box equipped with a temperature control system and surrounded by 16 58 W UV-C fluorescent lamps.

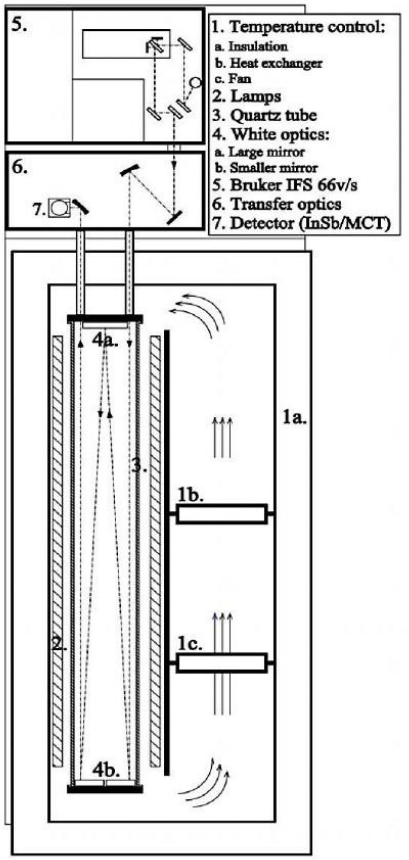

Figure 4.3 The photochemical reactor at CCAR.
(Source: Nilsson et al., 2009a)

The compounds were studied under atmospheric conditions and were therefore mixed in synthetic air (80 % N_2, 20 % O_2), at 700 ± 10 torr and 298 ± 5 K. The sample was irradiated with all UV-C lamps and scanned 128 times.

4.3.2 Experimental Procedure

The relative rate method was used to study the reaction of furan, 2,3-DHF and 2,5-DHF with Cl following the reactions:

$$\mathrm{CE} + \mathrm{ref} + \mathrm{Cl_2} \xrightarrow{h\nu} \mathrm{products} \qquad \text{R4.1a}$$

$$\mathrm{CE} + \mathrm{ref} + \mathrm{CH_3COCl} \xrightarrow{h\nu} \mathrm{products} \qquad \text{R4.1b}$$

were propane (C_3H_8), propene (C_3H_6) and cycloheptene (c-C_7H_{12}) where used as reference compounds, for $k_{\mathrm{ref+Cl}}$ see Appendix B. Cl_2 and acetyl chloride (CH_3COCl) were used as sources of free chlorine radicals, released via photo dissociation, $h\nu$.

All chemicals were retrieved from Sigma-Aldrich with a purity ≥ 97 %. The liquid samples were further purified using freeze–pump–thaw–cycling before initiating the experiments.

The compounds were introduced to the smog chamber via a gas handling manifold. The chamber and manifold are connected to vacuum pumps resulting in a pressure gradient allowing the compound to flow from the sample tube, through the manifold into the smog chamber. The manifold contains a reference volume of 0.5 litres which was used to determine the partial pressure of the sample being injected to the chamber. The effect of the vacuum pump is enhanced by emptying the manifold between experiments via a liquid nitrogen cooled cold trap. The compounds were injected to the chamber in the following order; reference compound, cyclic ether and chlorine source followed by a stream of synthetic air to fill the chamber to 700 *torr*.

The sample was irradiated by all 16 UV-C lamps in intervals of 70-100 seconds followed by 128 scans. Each spectrum was analysed using the spectrum subtraction function in *OPUS*, comparing the recorded spectrum with an initial reference spectrum. The procedure was repeated until 50 % of the initial furanic concentration remained.

4.4 Ozone Kinetic Experiments

Ozone experiments were carried out in the photoreactor at the Department of Chemistry, University of Oslo, following the relative rate method.

4.4.1 Experimental Setup

The photoreactor consists of a cylindrical 250 L electropolished stainless steel smog chamber connected to a Vacuum FTIR spectrometer (Bruker IFS 88). It is equipped with a White-type multiple reflection mirror system resulting in a 120 m optical path length (D'Anna et al., 2005). IR spectra are recorded by an Indium Antimonide (InSb) photodiode detector with the resolution set to be 0.5 cm^{-1} (determined by the spectrometer).

The compounds were studied under atmospheric conditions and were therefore mixed in synthetic air (20 % O_2, 80 % N_2) at 750 ± 10 torr, 298 ± 2 K and scanned 32 and 128 for DHF and furan respectively.

4.4.2 Experimental Procedure

The relative rate method was used to study the furanic reaction of furan, 2,3-DHF and 2,5-DHF with ozone following the reaction:

$$\mathrm{CE} + \mathrm{ref} + \mathrm{C_6H_{12}} + \mathrm{O_3} \rightarrow \mathrm{products} \qquad \text{R4.2}$$

were ethene (C_2H_4) and *iso*-butene (C_4H_8) where used as reference compounds. Cyclohexane (C_6H_{12}) was included as an OH scavenger to prevent unwanted reactions as alkane ozonolysis are expected to produce OH (Nilsson et al. 2009b). Cyclohexane follows the same OH initiated tropospheric chemical reactions as all hydrocarbons:

$$\mathrm{C_6H_{12}} + \mathrm{OH} \xrightarrow{\mathrm{M}} \mathrm{C_6H_{10}O} + \mathrm{HO_2} \qquad \text{R4.3}$$

For a more detailed reaction mechanism see Figure A5 in Appendix A5 – Tropospheric Chemistry. Since R4.3 produces cyclohexanone ($C_6H_{10}O$) together with hydroperoxyl radicals (HO_2) both compounds needs to be considered during the product study. High resolution reference spectrum of cyclohexanone was obtained from previous work produced in the same laboratory (Graham, 2013).

All chemicals were retrieved from Sigma-Aldrich with a purity ≥ 97 % and were further purified using freeze–pump–thaw–cycling before initiating the experiments.

Ozone was produced in a stream of oxygen passing through a corona discharge ozone generator (from Ozomax Inc.) connected to a tube filled with silica gel. The tube was placed cooling bath, resulting in temperatures low enough (EtOH + dry ice, ~ 200 K) for ozone to condense onto the silica gel.

The compounds were introduced to the smog chamber via a gas handling manifold in the same manner as to the photoreactor at CCAR (see Chapter 4.3.2). However, the cold trap was excluded for safety reasons; when ozone becomes liquid at these low temperatures its reaction with VOC is explosive. The compounds were injected to the chamber in the following order; cyclic ether, reference compound, cyclohexane and ozone followed by a stream of synthetic air to fill the chamber to 750 *torr*.

The ozone sample tube was first connected to the manifold under cooled conditions in order to remove all excess oxygen; the procedure was repeated as long as the internal pressure in the manifold rose rapidly. Once the tube only contained ozone it took roughly 10 minutes to fill the manifold with 40-60 torr ozone.

Due to the rapid nature of the reaction, see previous work by Graham (2013), the chamber was filled close to atmospheric pressures and repeated measurements were initiated before ozone was injected to the chamber. The furan ozonolysis was studied with 128 scans, repeated without interruption, while the DHF ozonolysis was even more rapid and therefore studied with 32 scans, repeated without interruption.

5 Product Study

This chapter presents the methodology of the product study performed during this project, which focused on the furanic ozonolysis mechanism. The study was initiated, and is based on, a comprehensive literature study (Figure 4.1:1) of the chemical reactions related to atmospheric ozonolysis, for more detailed atmospheric chemistry see Appendix A (Seinfeld & Pandis, 2006; Vereeken & Fransisco, 2012; Johnson & Marston, 2008; Monks, 2004). The present chapter begins with a short introduction to the chemical process of ozonolysis followed by a brief description of the experimental product study. The final section in this chapter describes the theoretical mechanistic study using computational methods.

5.1 The Ozonolysis Mechanism

The chemical process of ozonolysis, i.e. cycloaddition of ozone to hydrocarbon double bond, is an essential component in the tropospheric oxidation of VOC. It is a complex irreducible process considered to be a major source of OH in the troposphere (Johnson & Marston, 2008). The reaction results in an energetically unstable primary ozonide (POZ) which rapidly decomposes through O–O bond scission into a carbonyl compound and a biradical, referred to as the Criegee intermediate (CI), illustrated in Figure 2.5. In cyclic unsaturated compounds, such as furans, the O–O scission acts ring opening, resulting in a compound with both carbonyl- and CI characteristics.

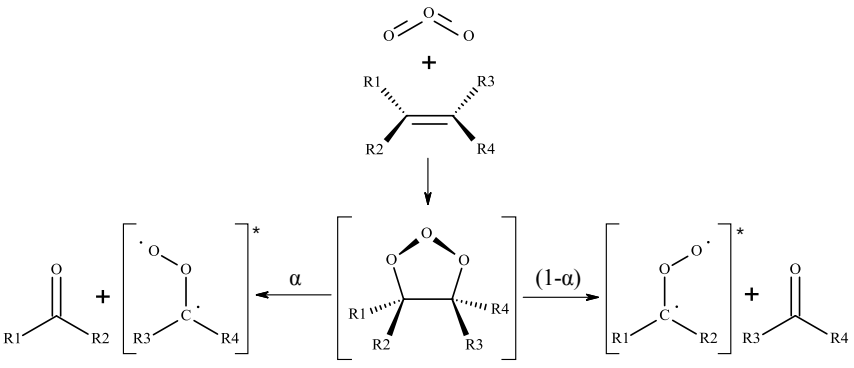

Fig 5.1 Ozonolysis is initiated by cycloaddition of ozone to an alkene double bond. The result is a primary ozonide which rapidly decomposes into a carbonyl and an energy rich Criegee intermediate. (Johnson & Marston, 2008)

The POZ formation is highly exothermic, releasing large amounts of energy, 50-60 kcal mol^{-1}, and is followed by low activation barrier < 20 kcal mol^{-1} making it decompose rapidly, making POZ undetectable under normal experimental conditions (Johnson & Marston, 2008). The CI formation results in second exothermic reaction sequence, releasing energies > 90 kcal mol^{-1}, compared to the initial reactants (Johnson & Marston, 2008).

CI resulting from larger compounds, e.g. CE, may stabilize by distribution of the excess energy over the whole molecule, while smaller CI follows one out of three decomposition channels:

1. If a suitable hydrogen atom is available CI may follow the *Hydroperoxide Channel* through a 1,4H-shift forming a hydroperoxide, which may be further decomposed to produce OH.

2. CI may cyclise, forming a dioxirane. As the ring splits up into a bis-oxy radical it finally forms an ester, and is therefore referred to as the *Ester Channel*. This channel is estimated to produce CO_2 through additional decomposition steps.

3. The *Stabilization Channel* includes a third body to which the CI loses its excess energy trough collision. The stabilized CI (SCI) may form a secondary ozonide, SOZ, through cyclisation. Additionally SCI can take part of bimolecular reactions, with for example other SCI or water molecules (Okumara, 2015).

5.2 Experimental Product Study

The product study is based on an analysis of furanic ozonolysis reaction spectra previously recorded by Graham (2013) at the Department of Chemistry, University of Oslo. The analysis was initiated by identification of all known peaks by comparison with a set of reference spectra. The reference spectra included the reactants (ozone + furans), cyclohexane which was included as an OH scavenger, background components such as water and obvious products, i.e. CO and CO_2. The remaining unknown peaks were considered belonging to the reaction products. These peaks were be further studied, see Chapter 5.2.1, and compared with an additional list of reference spectra (Figure 4.1:4a). It contained spectra of common air pollutants and compounds which have been suggested as furanic combustion product, see the in Appendix C – List of Studied Reference Spectra.

Once identified the reaction products was quantified (Figure 4.1:4b) using high resolution reference spectra as input in *MALT 5* (Multi-Atmospheric Layer Transmission). It is a non-linear least squares algorithm which generates a fitted synthetic spectrum, using a set of reference spectra of known molecular concentrations, to the experimental spectrum (Griffith, 1996). Reference spectra were either retrieved from the HITRAN (High Resolution Transmission) database (Rothman et al., 2009), containing 42 of the most commonly studied atmospheric compounds, or recorded during the experimental session. *MALT 5* includes the parameters path length, pressure and temperature in the calculation together with instrumental properties such as spectral shift and resolution.

5.2.1 Characteristic Group Frequencies

Experimental product spectra were evaluated based on reference spectra together with the knowledge on general shape and specific peaks resulting from particular functional groups. This section presents a brief description of some functional groups and their absorption characteristics.

IR absorption spectra can be divided in two regions, were the region below 1500 cm^{-1} is generally referred to as the *fingerprint region* due to the skeletal vibrations of the molecule (Banwell & McCash, 1994). Adding or changing a substituent in the molecular structure results in a distinct change in the absorption pattern, which is why this region is usually used to confirm potential products using high resolution reference spectra.

The region above 1500 cm^{-1} contains information about the functional group vibrations, presented in Table 5.1 – 5.2. Vibrational modes of functional groups arise from vibrations of individual molecular bonds, such as stretching and bending. The frequency of a vibrational stretch depends on the atomic masses together with the strength of the bond. The vibrational frequency increases with the strength of the bond (between similar atoms), i.e. C=C vibrate at higher frequencies than C–C, while decreases with the atomic mass, e.g. absorption spectra of chlorinated hydrocarbons are shifted to lower frequencies.

As IR absorption requires that the vibrational modes result in a change in the molecular dipole moment, centrosymmetric compounds, such as O_2 and Cl_2, will not be IR-active (Engel, 213). The more polar a molecule becomes, the more intense the corresponding absorption peak will be.

Carbonyl compounds usually obtain very sharp and intense absorption bands in the region between 1600-1750 cm^{-1}, see table 5.2. Larger compounds are related to broader absorption peaks due to the increased number of potential interatomic interactions. When molecules contain functional groups with similar absorption bands, resonance will occur and the frequencies may be shifted. An example is how the characteristic absorption bands for acid anhydrides are shifted toward higher frequencies compared to the other carbonyl groups in Table 5.2.

Table 5.1 Functional groups and their absorption frequencies. Unsaturated compounds usually vibrate at higher frequencies in the reported absorption bands. (Williams & Fleming, 1995)

Group	Structure	Band (cm^{-1})	
Carbon dioxide	O=C=O	2349	
	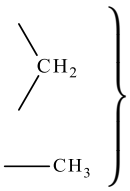	1470-1430	C-H deformation.
		1390-1370	Symmetrical deformation.
Alcohol	R-OH	1410-1260 1150-1040	O-H bending. C-O stretching.
Ether R_1OR_2	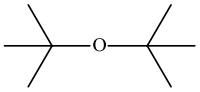	1150-1070	C-O stretching.
	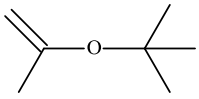	1275-1200 1075-1020	
Alkenes	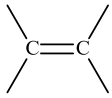	1680-1620 ~1625	When conjugated in aromatic rings, more intense than unconjugated double bonds.
Allenes	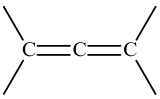	1950-1930	
Ketens	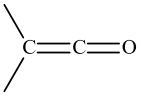	2155-2130	Very sharp.

Table 5.2 Carbonyl groups and their absorption frequencies. Unsaturated compounds usually vibrate at higher frequencies in the reported absorption bands, except for acid anhydride in which the unsaturated compound vibrate at lower frequencies, marked separate in the table. (Williams & Fleming, 1995)

Group	Structure	Band (cm^{-1})	
Aldehyde RHO	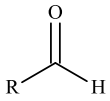	1740-1665	
Keton $R_1C(O)R_2$	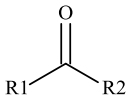	1725-1665	Often two bands when αβ-Unsaturated
		1750-1740	Five-ring ketones.
	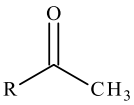	1360-1355	High intensity bands that dominates the region.
Carboxylic Acid R-C(O)OH	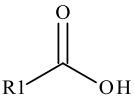	3000-2500	O-H stretching.
		1725-1690	
Esters and Lactones R_1-C(O)-O-R_2	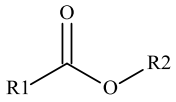	1750-1715 1780-1740	
		~1800	Bγ-Unsaturated five-ring lactone
	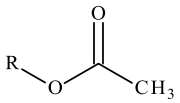	1385-1365	High intensity bands that dominates the region.
Acid Anhydrides R_1-C(O)-O-C(O)-R_2	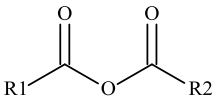	1850-1800 1790-1740	Two bands usually separated by 60 cm^{-1}. In cyclic compounds the lower band is most intense while in acyclic compounds the higher band most intense.
		1870-1820 1800-1750	αβ-Unsaturated.
		1870-1820 1800-1750	Saturated five membered ring.
		1300-1050	One or bands due to C-O stretching.

5.3 Theoretical Mechanistic Study

Ozonolysis is one of the most complex atmospheric chemical processes and the multistep reaction results in a set of highly energetic, experimentally undetectable intermediates. In this project, computational methods (Figure 4.1:3a) have been used in order to study the furanic ozonolysis mechanism. In Chapter 4.1 the reader became familiar with the third order reaction related to atmospheric chemistry; the following section will present a brief description of the well-established *Transition State Theory* (TST) of the chemical kinetics of bimolecular reactions followed by a description of the computational methodology.

5.3.1 Transition State Theory

According to the *Collision Theory* chemical reactions can be described as the collision of impenetrable, structureless spheres, kind of like billiard balls (Seinfeld & Pandis, 2006). In most cases this approach is too simple, especially for larger VOC which comes in various shapes and sizes.

In the product study performed during this project TST has been adopted when describing the bimolecular reaction of furanic ozonolysis. According to TST a molecular reaction occurs when two compounds collide resulting in a rearrangement of atoms and bonds in between the compounds (Seinfeld & Pandis, 2006). As the reactants, A and BC, move closer the molecular electron clouds starts to interact, repelling each other and the energy rises, as illustrated in Figure 5.2. If the force of the collision is sufficiently high the reactants overcome this energy barrier moving closer forming a A–B bond while breaking the B–C bond.

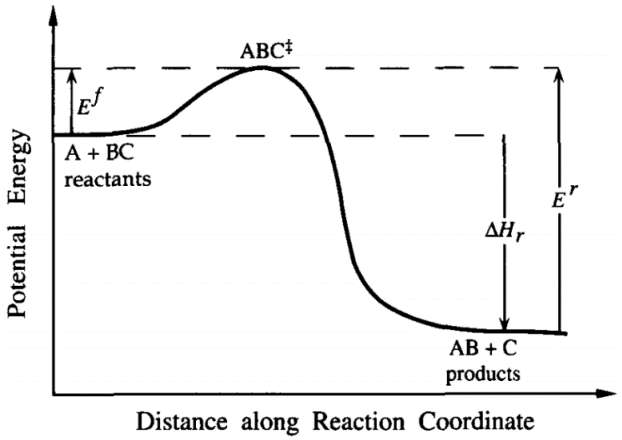

Figure 5.2 Energy diagram describing the reaction A + BC → AB + B were the y-axis represents the total potential energy of the reactants and the x-axis describes the reaction coordinate (Source: Seinfeld & Pandis, 2006)

At the top of the potential energy surface (PES) the activated reaction complex reaches its maximum energy, called the transition state (TS, denoted $ABC^{\ddagger}$ in Figure 5.2), which is in equilibrium with its reactants (Gross & Jørgensen, 2008). At this point the reaction can move forward or decay back into the reactants, which is assumed to be most likely according to TST.

The rate of the reaction is related with the activation barrier, see E^f in Figure 5.2. During a reaction involving a high activation barrier few of the molecular collisions results in activated complexes and the reaction progresses slowly. At atmospheric temperatures reactions involving two stable molecules are considered negligible due to the large energy barrier involving the electron rearrangement. Instead, atmospheric chemistry usually involves reactions were A is a radical and BC being a molecule, since the A–B bond forms almost instantaneously as the B–C bond breaks. The reaction becomes exothermic when the activated complex passed the TS and energy is released due to the new formed A–B bond.

A multistep reaction, such as ozonolysis, see Figure 5.3, is associated with more than one activation barrier resulting in reaction intermediates, e.g. CI. The intermediates may obtain higher internal energies than the sum of the initial reactants. However, it is necessary that the overall energy difference between the reactants and final products is negative, i.e. being exothermic, in order for the reaction to proceed forward (McMurry, 2011).

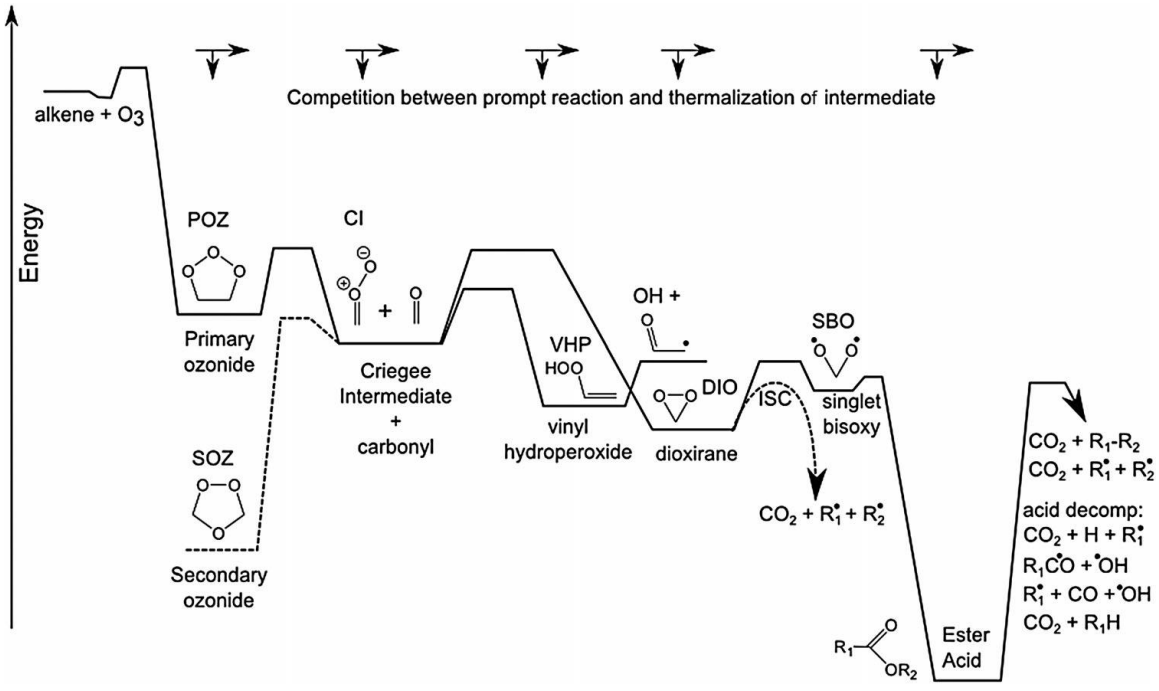

Figure 5.3 PES describing energy release during general alkenes ozonolysis.
(Source Vereecken & Fransisco, 2012)

5.3.2 Computational Chemistry

As TS can never be isolated or observed using experimental methods, computational chemistry becomes convenient when studying reaction mechanisms, e.g. ozonolysis. In this project the *reaction path method* has been applied in order understand the differences in the furanic ozonolysis. This method utilizes computational chemistry to obtain the stabilised geometries of stationary molecular structures, i.e. TS and intermediates, following the reaction pathway (Gross & Jørgensen, 2008).

Computational Chemistry is the combination of a theoretical procedure, e.g. the *Density Functional Theory* (DFT), called the level of theory and a basis set, which is a mathematical representation of the atomic orbitals (AO) (Foresman & Frisch, 1996). The accuracy of the calculations is increased with the level of theory and size of the basis set. It performs:

1. Energy calculation of molecular structures and activation barriers.
2. Geometry optimisations in order to find the structure with lowest energy, hence all structures are stabilised.
3. Calculation of molecular vibration spectra, which needs to be corrected with a scale factor before used (Alecu et al., 2010).

I this project the furanic ozonolysis have been studied using structure optimization and vibrational frequency calculations performed in *Gaussian 09*. The structures were first evaluated using RHF/3-21G (level of theory / basis set) followed by a more accurate calculation using M062X/Aug-CC-pVTZ.

TS was identified by scanning the stretching of specific bonds until breaking, i.e. reaches the top of a PES. TS is characterised by one of the vibrational frequencies being imaginary, whereas for a local minimum all vibrational frequencies are real (Gross & Jørgensen, 2008). The final result of the computational study was presented as a PES, facilitating the mechanistic study of the atmospheric furanic ozonolysis.

PART III – RESULTS

Part III presents and discusses the results of the project. Chapter 6-7 presents the results of the relative rate- and the mechanistic studies respectively. Chapter 8 discusses the atmospheric implications of the three furans and concludes the project.

6 Relative Rate Studies

Relative rate experiments have been performed under atmospheric conditions in smog chambers at CCAR, University of Copenhagen and Department of Chemistry, University of Oslo. This chapter begins by presenting the results of the chlorine- and ozone kinetics in separate sections followed by a section discussing the atmospheric furanic reactivity in contrast to similar compounds.

6.1 Chlorine Kinetics

The reaction of Cl with furan, 2,3-DHF and 2,5-DHF was investigated. Both the furan- and 2,5-DHF – Cl reaction rates were investigated using propene (C_3H_6) and propane (C_3H_8) as references compounds, see Appendix B for the reference rate constants. Experiments including each reference were performed twice resulting in four experiments in total for furan and 2,5-DHF. Corresponding relative rate plots are presented in Figure 6.1 and the corresponding slopes, i.e. k_{rel}/k_{ref}, are presented in Table 6.1 together with the rate constants related with each experiment.

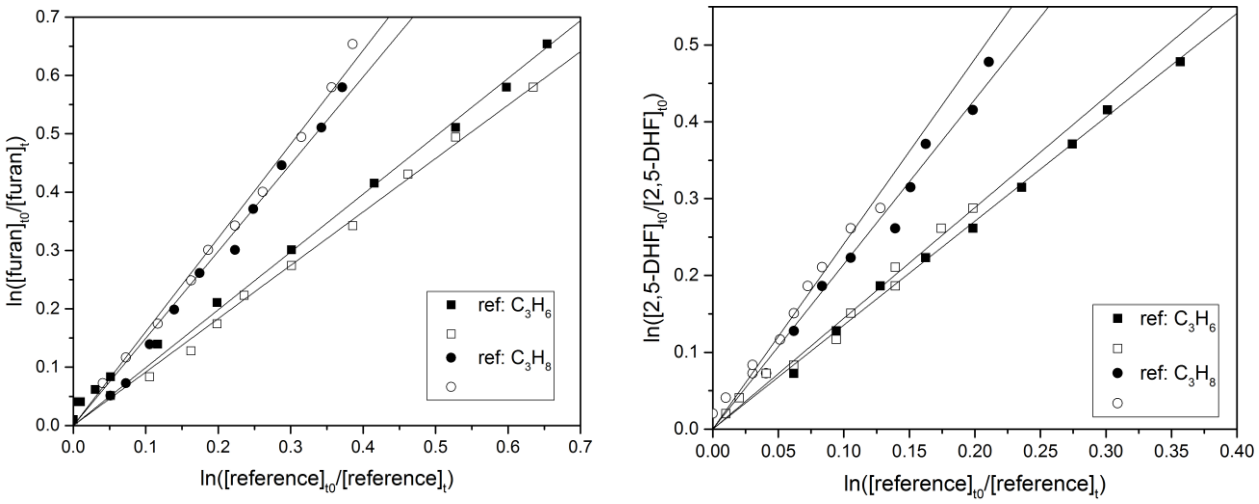

a) b)

Fig. 6.1 Relative rate experiments for Cl and a) furan and b) 2,5-DHF with propene (C_3H_6) and propane (C_3H_8) as references.

Table 6.1 Experimental reaction rate constants, k_{Cl}, for Cl reaction with furan, 2,3- and 2,5-DHF respectively, presented together with previous data. The error bars include the uncertainty of the slope together with the uncertainties in the reference rate constants, see Appendix B.

				$k_{Cl} \cdot 10^{10}$ ($cm^3\,molec^{-1}\,s^{-1}$).	
Chlorine exp.	Reference	Cl-source	k_{rel}/k_{ref}	Experimental	Literature
Furan	C_3H_6	Cl_2	0.99 ± 0.02	2.66 ± 0.13	
	C_3H_6	Cl_2	0.92 ± 0.01	2.45 ± 0.10	
	C_3H_8	Cl_2	1.49 ± 0.03	2.09 ± 0.10	
	C_3H_8	Cl_2	1.61 ± 0.02	2.25 ± 0.10	
			mean	**2.36 ± 0.11**	2.0 ± 0.2 [1]
2,3-DHF	C_3H_6	CH_3COCl	2.88 ± 0.15	7.73 ± 0.65	
	cyclo-C_7H_{12}	CH_3COCl	1.28 ± 0.03	6.57 ± 0.86	
			mean	**7.15 ± 0.75**	4.52 ± 0.99 [2]
2,5-DHF	C_3H_6	Cl_2	1.44 ± 0.03	3.86 ± 0.20	
	C_3H_6	Cl_2	1.35 ± 0.01	3.63 ± 0.14	
	C_3H_8	Cl_2	2.41 ± 0.06	3.37 ± 0.19	
	C_3H_8	Cl_2	2.15 ± 0.05	3.00 ± 0.16	
			mean	**3.47 ± 0.17**	4.48 ± 0.59 [2]

[1] Cabañas et al., 2005.
[2] Alwe et al., 2013.

In the 2,3-DHF – Cl experiments, Cl_2 could not be used as a source of free chlorine radicals as it showed instantaneous dark reaction with 2,3-DHF. According to the literature both DHF reacts with Cl_2 in the dark (Alwe et al, 2014). Furan and 2,5-DHF was left in the chamber for 20 and 40 minutes respectively without revealing any significant dark reaction. The dark reaction of furan and 2,5-DHF with Cl_2 could therefore be neglected during the time limit of the experiments.

Instead, acetyl chloride (CH_3COCl) was used as the source of free chlorine radicals in the relative rate experiments with 2,3-DHF. As acetyl chloride absorbs in the infrared wavelength region, in contrast to Cl_2, the experimental spectra includes additional peaks compared to the previous Cl experiments. It was therefore necessary to find reference compounds with characteristic absorption bands in the remaining wavelength windows. The 2,3-DHF reactions with chlorine radicals were performed using two different reference compounds, i.e. propene (C_3H_6) and cycloheptene (C_7H_{12}). Figure 6.2 presents the relative rate plot of the two 2,3-DHF experiments and the corresponding slopes, i.e. k_{rel}/k_{ref}, is presented in Table 6.1 together with the rate constants related with each experiment. Ideally, these experiments should have been performed twice in order to establish reproducibility, but unfortunately there was no time left in the laboratory.

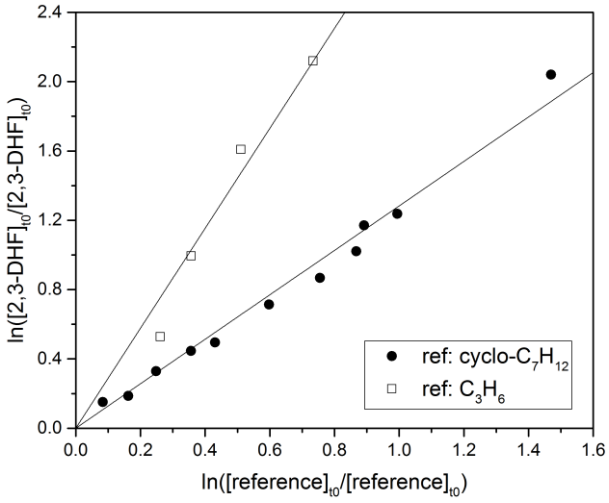

Fig. 6.3 Relative rate experiments for chlorine radicals and 2,3-DHF with propene (C_3H_6) and *cyclo*-heptene (C_7H_{12}) as references.

The final rate constants describing the Cl reaction with furan, 2,3- and 2,5-DHF is presented in bold letters in Table 6.1 as the mean of the experimental rate constants for the respective reaction. The error bars include the uncertainty of the slope together with the uncertainties in the reference rate constants. The furan reaction rate constant is consistent within the error margins of the data previously determined by Cabañas et al. (2010). The 2,5-DHF rate constant indicate a slightly slower reaction while the 2,3-DHF rate constant is considerably faster compared to the data determined by Alwe et al. (2013).

6.2 Ozone Kinetics

The reaction of ozone with furan, 2,3-DHF and 2,5-DHF was investigated. The reactions have previously been studied using the absolute rate method without good results due to experimental difficulties (Graham, 2013). Ethene (C_2H_4) and *iso*-butene (C_4H_8) were used as reference compounds for the ozone reaction with furan and 2,5-DHF respectively. The corresponding relative rate plots are presented in Figure 6.3 and the resulting slopes, i.e. k_{rel}/k_{ref}, are presented in Table 6.2 together with the rate constants related with each experiment.

During previous experimental studies the reaction of ozone with 2,3-DHF was found to proceed too fast in order to be studied using the absolute rate method (Graham, 2013). During this project the reaction was investigated once again, this time using the relative rate method, unfortunately, without any better results. Hence, the reaction of ozone with 2,3-DHF is too rapid in order to be studied with the available reference compounds in the present setup.

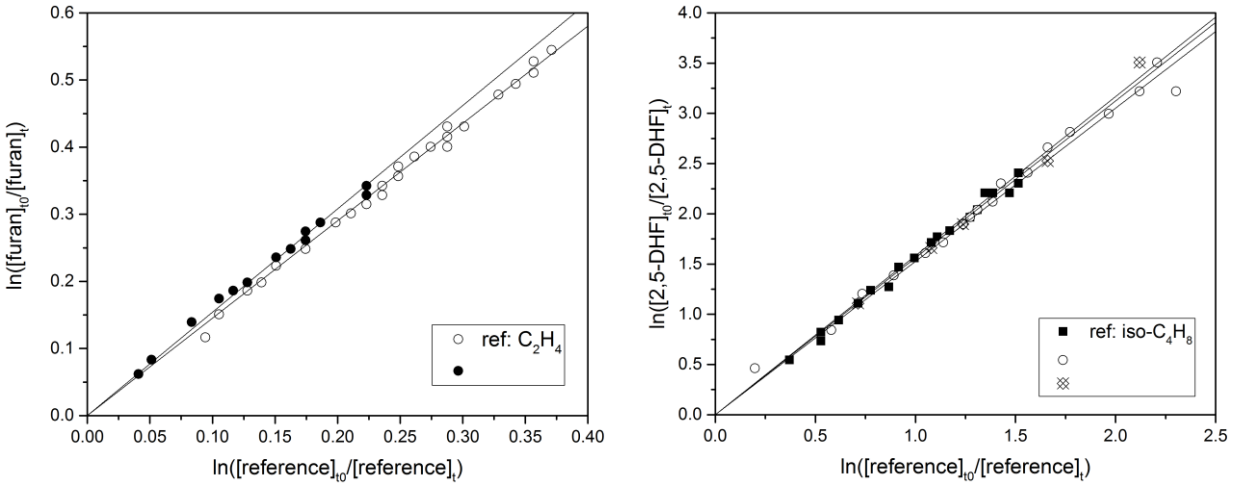

a) b)

Fig. 6.1 Relative rate experiments for ozone and a) furan and b) 2,5-DHF with ethene (C_2H_4) and *iso*-butene (*iso*-C_4H_8) as references respectively.

The final rate constants describing the ozone reaction of furan and 2,5-DHF is presented in bold letters in Table 6.2 as the mean of the experimental rate constants for respective reaction. The error bars include the uncertainty of the slope together with the uncertainties in the reference rate constants. The result of the two furan- and three 2,5-DHF experiments were consistent within the experimental error margins of the data determined by Graham (2013) and Alwe et al. (2014). The result is therefore considered to be reliable and no further experiments with additional reference compounds were performed.

Table 6.2 Experimental reaction rate constants, k_{O_3}, for O_3-reaction with furan, 2,3- and 2,5-DHF respectively, presented together with previous data. The error bars include the uncertainty of the slope together with the uncertainties in the reference rate constants, see Appendix B.

				$k_{O_3} \cdot 10^{17}$ (cm^3 molec^{-1} s^{-1})	
Ozone exp.	Reference	O_3-source	k_{rel}/k_{ref}	Experimental	Literature
Furan	C_2H_4	O_2	1.45 ± 0.01	0.232 ± 0.008	
	C_2H_4	O_2	1.54 ± 0.01	0.237 ± 0.010	
				mean **0.239 ± 0.009**	0.224 ± 0.037 [1]
2,5-DHF	*iso*-C_4H_8	O_2	1.58 ± 0.03	1.71 ± 0.08	
	iso-C_4H_8	O_2	1.56 ± 0.01	1.69 ± 0.06	
	iso-C_4H_8	O_2	1.53 ± 0.02	1.65 ± 0.07	
				mean **1.68 ± 0.07**	1.65 ± 0.3 [2]
2,3-DHF					443.2 ± 79.0 [2]

[1] Graham, 2013.
[2] Alwe et al., 2014.

6.3 Evaluation of Atmospheric Reactivity

The prior experimental study indicates that furan reacts slower with both Cl and ozone than the two DHF do. This can be explained by furans aromatic ring structure lowering its internal energy, and hence reactivity towards chlorine radicals and ozone compared to the two DHF.

The reaction of 2,3-DHF with Cl and ozone is more rapid than the corresponding 2,5-DHF reactions. This is in contrast to the literature which states that the DHF- chlorine reaction rates are very similar (Alwe et al., 2013). Relative rate experiments with Cl and 2,3-DHF needs to be reproduced in order to confirm this result. The relation of the furanic Cl- and ozone reaction is illustrated in Figure 6.4.

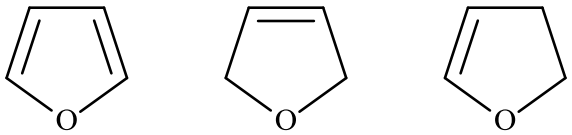

$$k_{\text{furan+Cl}} < k_{2,5-\text{DHF+Cl}} < k_{2,3-\text{DHF+Cl}}$$

$$k_{\text{furan+O}_3} < k_{2,5-\text{DHF+O}_3} < k_{2,3-\text{DHF+O}_3}$$

Figure 6.4 The chlorine- and ozone reaction rates increase with the saturation of the furan. Additionally the DHF reactivity depends on the position of the double bond.

There is an obvious trend for a slower furanic reaction with OH than with Cl when comparing the experimental result with rate constants for the OH reaction reported in the literature. The furanic OH reaction follows the same pattern as the Cl reaction, with furan reacting slower than DHF. According to the literature 2,3-DHF react faster with OH than 2,5-DHF do. As the atmospheric VOC reaction with Cl should progress in the same manner as the OH-reaction, see Chapter 2.2, this confirms the result that 2,3-DHF reacts more rapid with Cl than 2,5-DHF do.

Table 6.3 Comparison of the furanic reaction rate constants, *k*, with chlorine- and hydroxyl radicals.

	$k_{\text{Cl}} \cdot 10^{10}$ ($\text{cm}^3\,\text{molec}^{-1}\,\text{s}^{-1}$)	$k_{\text{OH}} \cdot 10^{10}$ ($\text{cm}^3\,\text{molec}^{-1}\,\text{s}^{-1}$)
Furan	2.36 ± 0.11	0.40 ± 0.03 [1]
2,3-DHF	7.15 ± 0.75	1.20 ± 0.28 [2]
2,5-DHF	3.47 ± 0.17	0.65 ± 0.17 [2]

[1] Atkinson et al., 1983.
[2] Alwe et al., 2014.

Table 6.4 Reaction rate constants, k_{O3}, for several cyclic compounds with different saturation and oxygen position. The reactivity against ozone increases downwards in the table, hence the reactivity towards ozone depends on the aromaticity, ring size and position of the oxygen.

Compound	Structure	k_{O_3} (cm^3 $molec^{-1}$ s^{-1})	Reference
Benzene	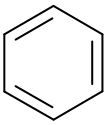	1.72×10^{-22}	Toby et al. 1985.
Furan	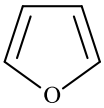	2.54×10^{-18}	*Present work.*
2,5-DHF	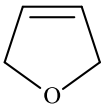	1.68×10^{-17}	*Present work.*
1,4-Cyklohexadiene	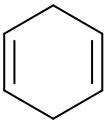	6.39×10^{-17}	Atkinson et al., 1983a.
Cyclohexene	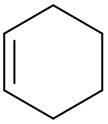	$1{,}04 \times 10^{-16}$	Atkinson et al., 1983a.
Cyclopentene	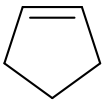	$2{,}75 \times 10^{-16}$	Atkinson et al., 1983.
2,3-DHP	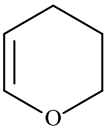	3.14×10^{-16}	Alwe et al., 2014.
1,3-Cyclohexadiene	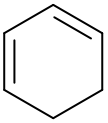	1.97×10^{-15}	Atkinson et al., 1983a.
2,3-DHF	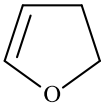	4.43×10^{-15}	Alwe et al., 2014.

The position of the oxygen in relation to the double bond affects the electronic structure of the DHF, and thus its reactivity. The molecular reactivity increases with the electron density as the electrons becomes more accessible for the reactant. This is especially evident when examining the DHF reactivity towards Cl_2, which is usually considered to be unreactive towards other compounds under atmospheric conditions. As 2,5-DHF did not show any significant dark reaction with Cl_2 it follows the general atmospheric chemical reactions, while 2,3-DHF actually do reacts with Cl_2. This may arise from the fact that free chlorine radicals attack hydrogen atoms, independent of the oxygen positon, while molecular chlorine interacts with the double bond π-electrons, therefore more dependent on the location of the oxygen versus double bond (McMurry, 2011).

When comparing literature data of the reactivity of ozone against several cyclic compounds it becomes evident that it is a complex chemical process, see Table 6.4. Cyclopentene reacts faster with ozone than furan and 2,5-DHF do, but slower than 2,3-DHF. Cyclopentene is experiencing ring strain, due to the fact that the bond angles are smaller than the ideal 109.5° (McMurry, 2011). It seems that the oxygen stabilizes the molecule when located opposite to the double bond, compared to cyclopentene. In contrast, DHF becomes more unstable than cyclopentene when the oxygen is located next to the double bond.

According to Atkinson (1983a) ozone reaction rates are enhanced by ring strain, this seems not to be the case with oxygenated cyclic compounds. Contrary, all these six membered rings (except benzene) reacts faster with ozone than both furan and 2,5-DHF. Additionally, cyclohexene is less reactive than 2,3-dihydroppyran (2,3-DHP) towards ozone. 1,3-cyclohexadiene is even more reactive towards ozone than 2,3-DHP, while 1,4-cyclohexadiene react even slower with ozone than cyclohexene do. The only compounds behaving as expected are furan reacting faster than benzene, which is slightly more aromatic and hence more stable than furan (McMurry, 2011).

The aromaticity, ring size and oxygen position does clearly affect the atmospheric reactivity of cyclic compounds, but needs to be further investigated in order to the fully understand the atmospheric process of ozonolysis of cyclic compounds.

6.3.1 Atmospheric Lifetimes

Atmospheric lifetimes of the three furans with respect to the Cl and ozone reactions have been determined, following Eq. 4.2, and compared to the literature data for the corresponding OH reactions.

Atmospheric lifetime in highly polluted urban areas was calculated using the ozone reference limit, 120 μg/m^3 ~ 60 ppb, established by the *EU Air Quality Objectives* and the upper Cl levels, which is estimated to be the same as in a maritime environment (EEA, 2014; Young et al., 2014). The corresponding atmospheric lifetimes in rural areas was calculated using the lower ozone and Cl levels reported in the literature (Seinfeld & Pandis, 2006; Young et al., 2014). Finally, the furanic atmospheric lifetimes with respect to the OH reaction were calculated using the global mean OH concentration (Seinfeld & Pandis, 2006). The resulting atmospheric lifetimes are presented in Table 6.5, in were the corresponding reactants concentrations are presented within brackets.

The results reveal that the shortest furanic atmospheric lifetimes are with respect to the OH reaction, especially in rural areas. The results indicate that the furans mainly decay through reaction with OH. The Cl reaction could become important in highly polluted areas, close to chlorine source, when the competition for the OH reaction increases due the high VOC levels, according to the tropospheric chemistry outlined in Appendix A5.

The furanic Cl reaction can be considered to be insignificant in rural areas due to atmospheric lifetimes exceeding 160 days. In rural maritime areas, where the chlorine concentrations are estimated to reach the same levels as in polluted urban areas, the furanic reaction with OH is still the most important due to the lower competition between furans and other VOC.

Table 6.5 Atmospheric lifetimes, τ, considering the ozone- and Cl concentrations in urban and rural areas, compared with a global estimate of the OH concentration. Concentrations are measured in molecules cm^{-3}.

	τ_{O_3}		τ_{Cl}		τ_{OH}
	Urban [1.5×10^{12}]	Rural [0.5×10^{12}]	Urban/Maritime [10^5]	Rural [10^2]	Global [10^6]
Furan	77.5 h	10 days	11.8 h	490 days	6.9 h [1]
2,3-DHF	—	—	3.9 h	162 days	2.3 h [2]
2,5-DHF	11.0 h	1.5 days	8.0 h	334 days	4.3 h [2]

[1] Using the rate constant determined by Atkinson et al., 1983.
[2] Using rate constants determined by Alwe et al., 2014.

7 Product Study

The prior laboratory study was combined with product studies focusing on the furanic ozonolysis. The product study is based on comprehensive analysis of reaction spectra recorded by Graham, 2013, together with theoretical calculations performed in *Gaussian 09*. This chapter, which presents the finding of the product study, is divided in three sections; the first takes a look at the experimental reaction spectra in order to identify and make a first assumption of potential pollutants related to the reactions. The second section proposes a decomposition mechanism for the ozonolysis of 2,5-DHF, based on the ozonolysis theory from the literature together with the findings in the first section. In the third and final section the first reaction steps during the ozonolysis of 2,3- and 2,5-DHF is compared using PES.

The cycloaddition of ozone to the three different furans are presented in Figure 7.1 together with the resulting CI. The product study has focused on 2,5-DHF as it is symmetrical and therefore resulting in just one CI, independent on were the O-O scission takes place. Once a final decomposition mechanism describing the ozonolysis of 2,5-DHF has been established its reaction pathways could be extended to furan and 2,3-DHF. Furthermore, Figure 7.1 reveals that the CI of furan and 2,3-DHF are identical except for the rate of saturation. The additional double bond in furan, compared to 2,3-DHF, makes the resulting CI less flexible which may affect the number of potential products.

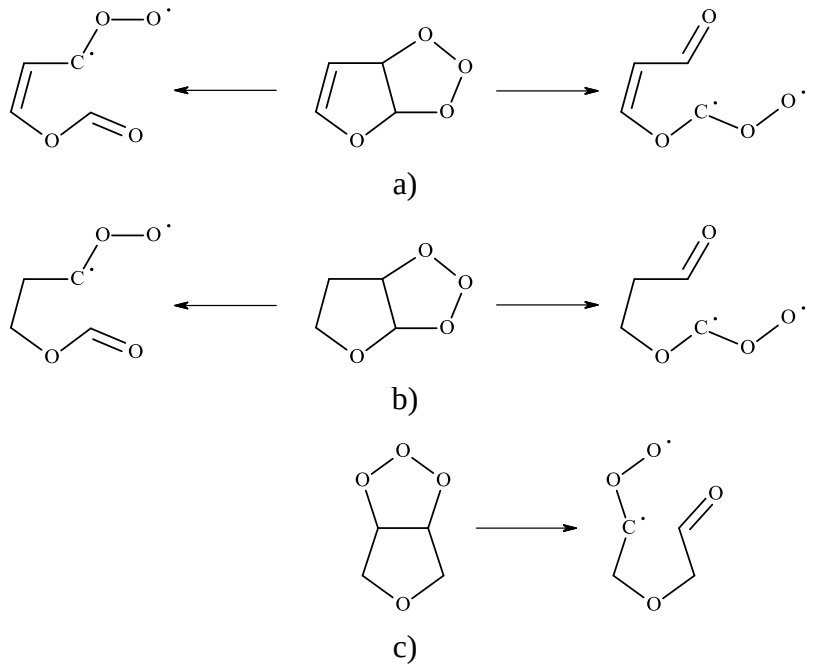

Figure 7.1 Ozonolysis of a) furan b) 2,3-DHF and c) 2,5-DHF.
Ozone adds to the double bond, resulting in a primary ozonide (POZ)
which rapidly splits up into an energetic Criegee intermediate (CI).

7.1 Experimental Results

FTIR reaction spectra recorded at the Department of Chemistry, University of Oslo, during spring 2013, have been studied in order to identify atmospheric pollutants related to the potential furanic biofuel (Graham, 2013). The analysis was initiated by identification of all known peaks by comparison with a set of reference spectra. The reference spectra included the reactants (ozone + CE), cyclohexane which was included as an OH scavenger, background components such as water and obvious reaction products, i.e. CO and CO_2. In atmospheric absorption spectra water appears as sharp, repetitively spikes, while carbon monoxide and carbon dioxide are recognised on their characteristic wing shaped absorption spectra in the region between 3000 and 2000 cm^{-1} (Graham, 2013). The remaining unknown peaks were considered belonging to the unknown reaction products.

The absorption peaks belonging to the furanic ozonolysis products appears mainly in two absorption regions, i.e. the carbonyl region, 1850-1600 cm^{-1} and the fingerprint region, 1400-1050 cm^{-1} (Williams & Fleming, 1995). It is possible that the products also absorb at wavenumbers < 1050 cm^{-1}, if so they could not be detected due to the strong absorption bands of ozone in this region. Additional absorption bands were observed at wavenumbers > 2000 cm^{-1}, but the analysis is restricted to the carbonyl- and fingerprint regions, as they include the necessary information needed to identify the potential reaction products, see Table 5.1-5.2.

Figure 7.2 presents reaction spectra for the ozonolysis of furan, 2,3- and 2,5-DHF recorded by Graham (2013) (were 0 is the initial scan used as reference spectrum when estimating the relative reactant decay between scans). The light grey spectra are the reference spectra for each of the reactants; excluding ozone as it does not display any strong absorption lines in these regions. These experimental absorption spectra were compared to a set of reference spectra in order to be confirmed or ruled out as potential reaction products. See the complete list of all evaluated reference spectra in Appendix C.

A distinct peak, growing around 1776 cm^{-1} in the carbonyl region, was identified in all three furanic reaction spectra. When paired together with the peak growing at lower wavenumbers around 1105 cm^{-1}, formic acid (HC(O)OH) could be identified as reaction product in the ozonolysis of all three furans. The reference spectra of formic acid is presented as a black spectrum in 2,3-DHF's reaction spectra in Figure 7.2. Additionally, formaldehyde (HC(O)H) could be identified in both 2,3- and 2,5-DHF while absent in the furan reaction spectra, see the dashed black reference spectra in 2,3-DHF's product spectra in Figure 7.2.

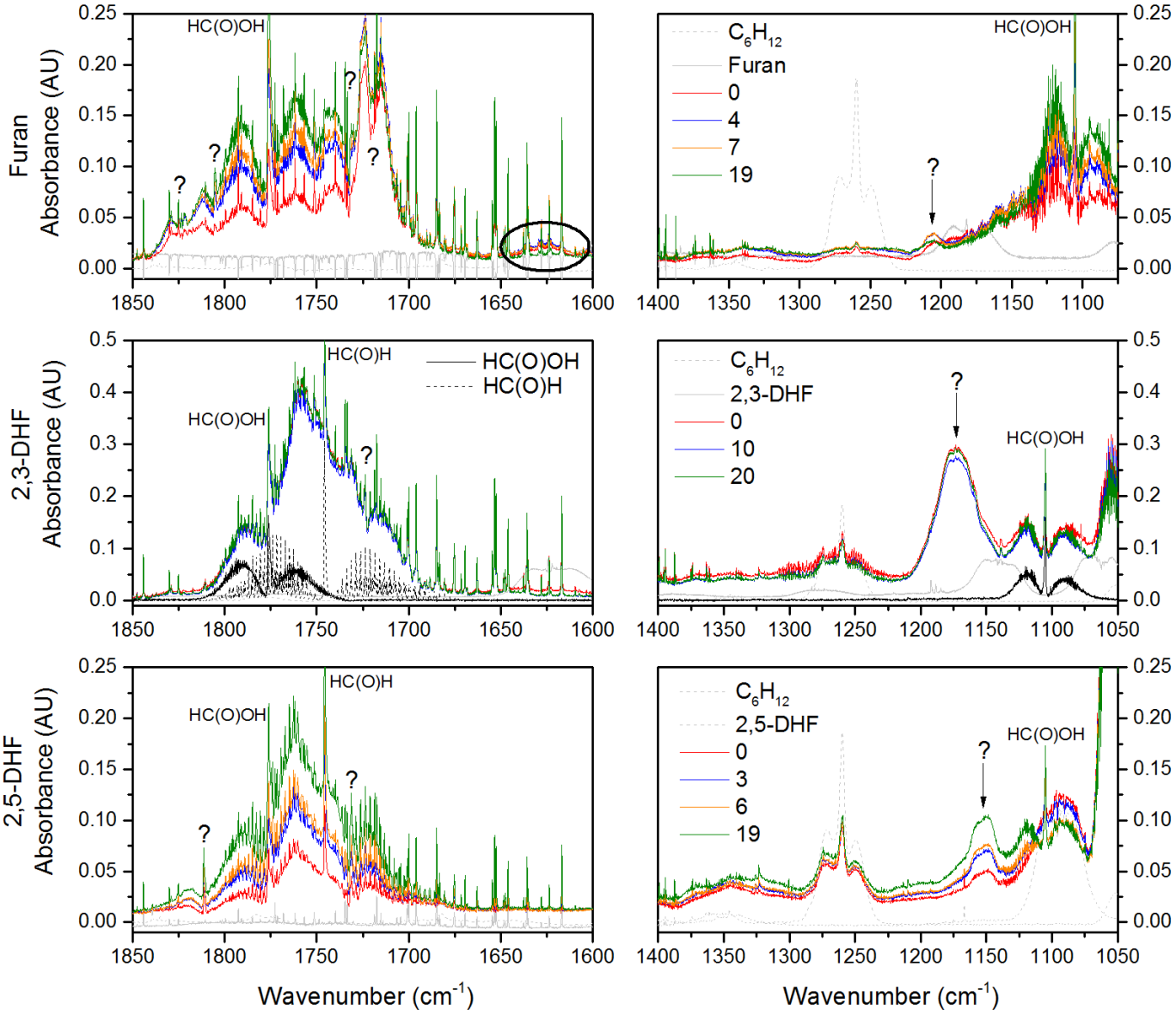

Fig. 7.2 Product spectra for Furan, 2,3- and 2,5-DHF respectively in the 1850-1600 and 1400-1075 cm^{-1}. The circled area and peaks marked with **?** denotes unknown products. (Source: Graham, 2013)
(Furan – 5th exp. 130425; 2,3-DHF – 2nd exp. 130425; 2,5-DHF – 3rd exp. 130424)

Furthermore, the furan reaction spectra include a broader peak, 1725-1700 cm^{-1}, which is not found in the two DHF product spectra. This broad peak is plotted in Figure 7.3a together with the reference spectrum for glyoxal obtained from Eurochamp reference data base (Eurochamp, n.d.). Due to the low resolution of the reference spectra it is not possible to say if it is a match, but the fact that glyoxal appear in the theoretically estimated furanic ozonolysis mechanism, see Chapter 7.2, strengthen the hypothesis that this is indeed Glyoxal.

Figure 7.3b presents a zoom in on the unknown reaction product in the spectral region marked with a black circle in Figure 7.2. In Figure 7.2 it appears that this product could be 2,3-DHF formed during the furan experiment, but in Figure 7.3b the product spectra and the 2,3-DHF reference spectrum does not match. However, due to the fact that this product is shifted compared to furans reference spectra it could actually be a furanic ring with a new substituent, see Chapter 5.2.1.

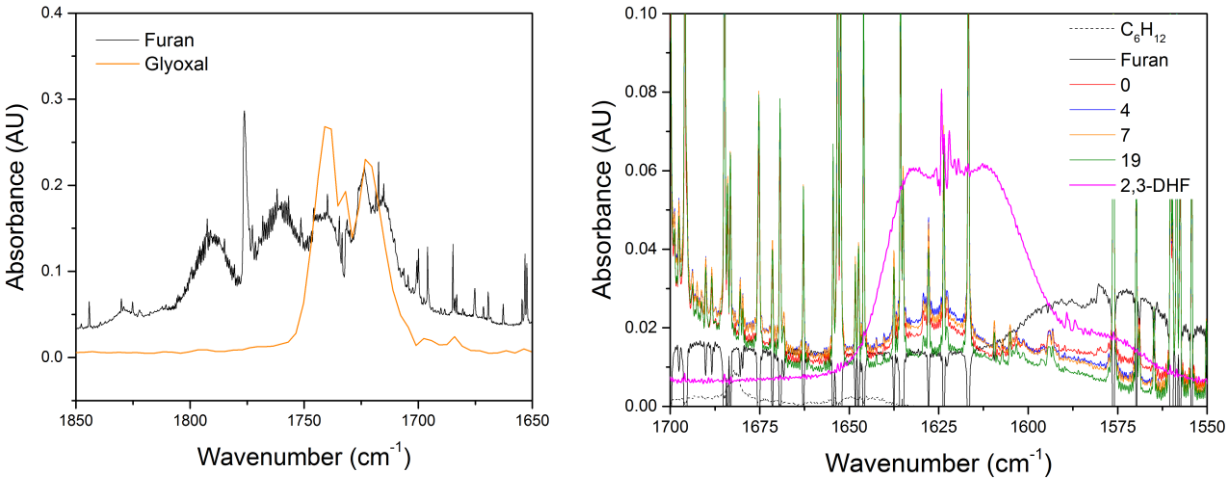

a) b)

Figure 7.3 Furan ozonolysis spectra together with:
a) Glyoxal (Eurochamp) and b) 2,3-DHF (Graham, 2013) reference spectrum.

Since no experimental reference spectra was available for the larger products potentially produced in the three different ozonolysis decomposition channels (*Hydroperoxide-, Ester- and Stabilisation Channel*), theoretical vibrational spectra were produced using *Gassian 09*. Unfortunately the quality of these spectra was to low and no conclusion could be drawn from them. Figure 7.4 presents the computational vibration spectrum of 2,5-DHF potential SOZ (calculated with RHF/3-21G). SOZ could be ruled out since the 2,5-DHF reaction spectra does not include any absorption lines in the same region as SOZ, see ~1200 cm^{-1}. For further results of the computational study see Chapter 7.2.2.

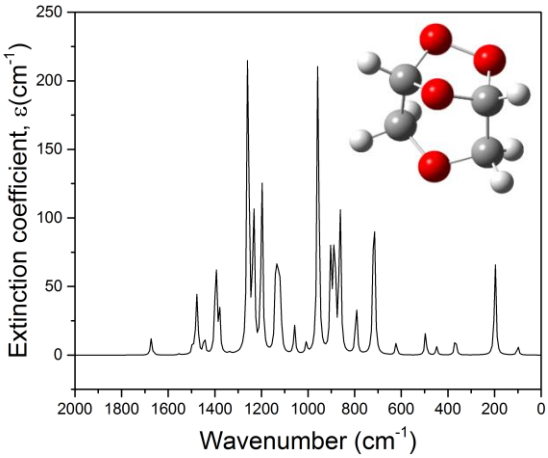

Figure 7.4 Computational vibration spectrum of the 2,5-DHF secondary ozonide.

The fact that the absorption in the carbonyl region results in a broader peak, shifted towards higher frequencies compared to the literature indicates on larger reaction products including several similar functional groups resulting in resonance, see Chapter 5.2.1. The number of potential products seems to decrease with the saturation, see number of unknown peaks marked in figure 7.2. This result contradicts the hypothesis that furan results in fewer ozonolysis products as a result of the less flexible CI. The majority of the unknown reaction products results in wing shaped absorption peaks, indicating on smaller molecules forming during the furanic ozonolysis.

The carbonyl region was further analysed by comparing the growth of the different peaks. This procedure could answer when different products are being formed, i.e. the order for the reactions to take place in the final mechanism. Figure 7.3b indicates on a product first being formed, see the growing peaks in the red – orange – blue spectrum, and then consumed, see the peak shrinking in the green spectrum. This part was combined with a quantification of the reactants and products throughout the steps of the experiments, using *MALT 5*. The result of the quantification analysis is presented in Figure 7.5, were a) and b) illustrates the ozone consumption and formic acid production during the furan experiments respectively, and c) and d) illustrates the ozone consumption and formic acid production during the 2,5-DHF experiments respectively.

Due to the rapid ozonolysis of 2,3-DHF, no quantification analysis could be performed for the reaction as all reaction products are being formed once the experiment is initiated, see Figure 7.2. Figure 7.5 indicates three phases in the furanic degradation, were the second phase seems to be a furanic reaction with an additional reactant, as the ozone concentration stabilised while the furanic concentration continued to decrease. Furthermore, the production of formic acid slowed down during the reactions second phase, indicating additional products being formed in the unknown furanic reaction.

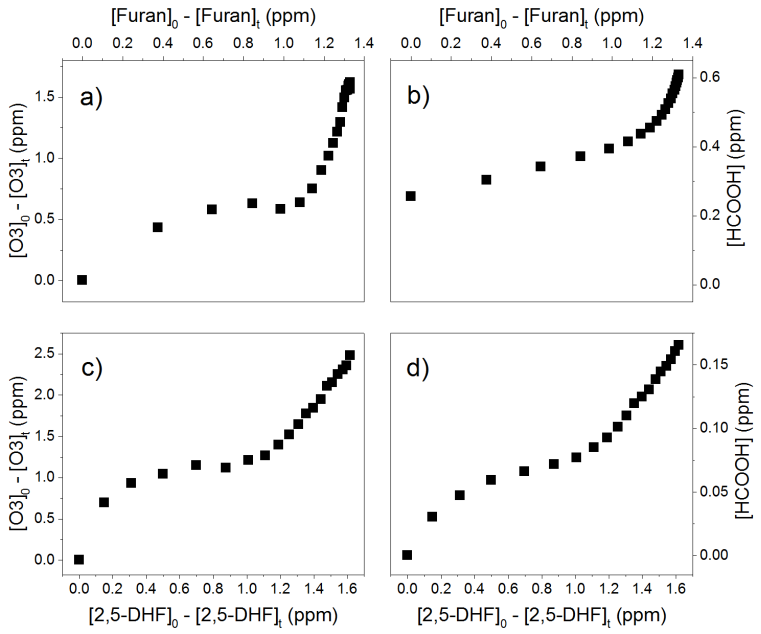

Figure 7.5 Ozone consumption plotted against the a) furan- and c) 2,5-DHF consumption, and formic acid production plotted against the b) furan- and d) 2,5-DHF consumption. (Furan – 5th exp. 130425; 2,5-DHF – 3rd exp. 130424)

Common alkene ozonolysis is expected to produce hydroxyl radical, OH, in a varying yield between 7-100 % (Monks, 2005). Cyclohexane was added to the experiments with the purpose to scavenge any produced OH, preventing it to react with the furans. Due to the fact that the experiments were faster than expected (Graham, 2013), and that barely any cyclohexane was consumed there is a possibility that produced OH actually did react with the furans, as a result more rapid furanic reaction than cyclohexane reaction. In order to get an idea of the importance of the OH reaction some simple calculations were executed. It was assumed that the OH reaction can be considered to be insignificant as long as the rate of ozonolysis is at least one hundred times larger than the rate of the OH reaction. As the experimental ozonolysis rate is known it is possible to determine at what concentrations the OH reaction would become important.

Table 7.1 Required concentrations for OH to be a significant competitor to the ozonolysis of furans, were the concentrations are measured in molecules cm^{-3}.

	Furan	2,3-DHF	2,5-DHF
$[O_3]$	$\sim 10^{15}$	$\sim 10^{16}$	$\sim 10^{14}$
[OH]	$\sim 10^{6}$	$\sim 10^{9}$	$\sim 10^{5}$

The result indicates that even a small production of OH could be significant for the furanic OH reaction to occur and actually outcompete the furanic ozonolysis. This information will be helpful when designing new furanic ozonolysis experiments aimed to determine the rate constants and the associated reaction mechanisms.

7.2 DHF Ozonolysis Mechanism

The atmospheric ozonolysis of alkanes is a well-established process described in Chapter 5.1 (Vereecken & Fransisco, 2012). The present chapter presents the results when applying the general ozonolysis mechanism to the symmetric, saturated ether, namely 2,5-DHF. The literature suggests ozonolysis of cyclic compounds to form SOZ, but it was excluded as a stable product in Chapter 7.1. In highly polluted environment, such as the experimental chamber, the stabilized CI may collide with other stabilized CI, resulting in oxygen and possibly 2,2-Oxydiacetaldehyde, but this reaction is unlikely to occur in the atmosphere even during severe ozone episodes. Finally it has been suggested that CI could interact with water and water dimers forming peroxides (Okumara, 2015).

According to the theoretical calculations performed within the present work, see section 7.2.1, CI's energy is sufficiently high to vibrate and decompose before it had time to stabilise through collision with another compound, i.e. the vibration energy is larger than the rate of collision. This suggest that the 2,5-DHF ozonolysis mechanism follows the Hydroperoxide- or Ester channel, see Figure 7.6. Based on this hypothesis further decomposition following the two channels have been evaluated, see Figure 7.7.

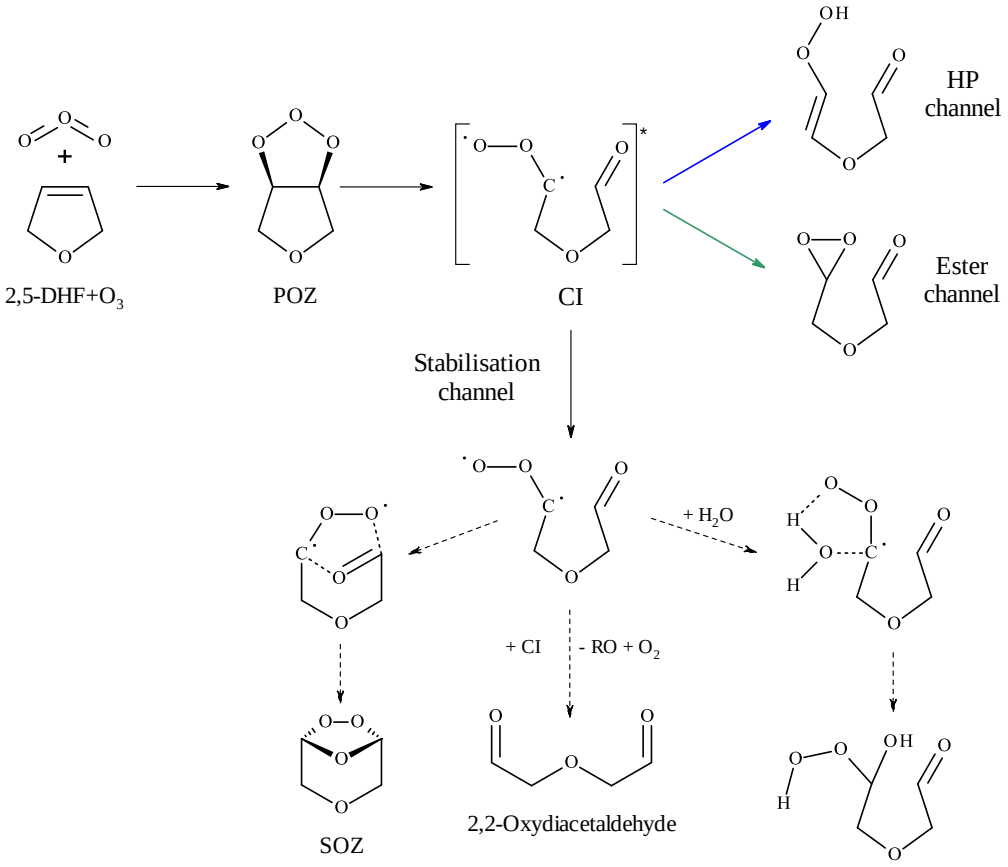

Figure 7.6 Proposed decomposition mechanism of the 2,5-DHF Criegee Intermediate. The blue and green arrow refers to the corresponding transitions states in Figure 7.9.

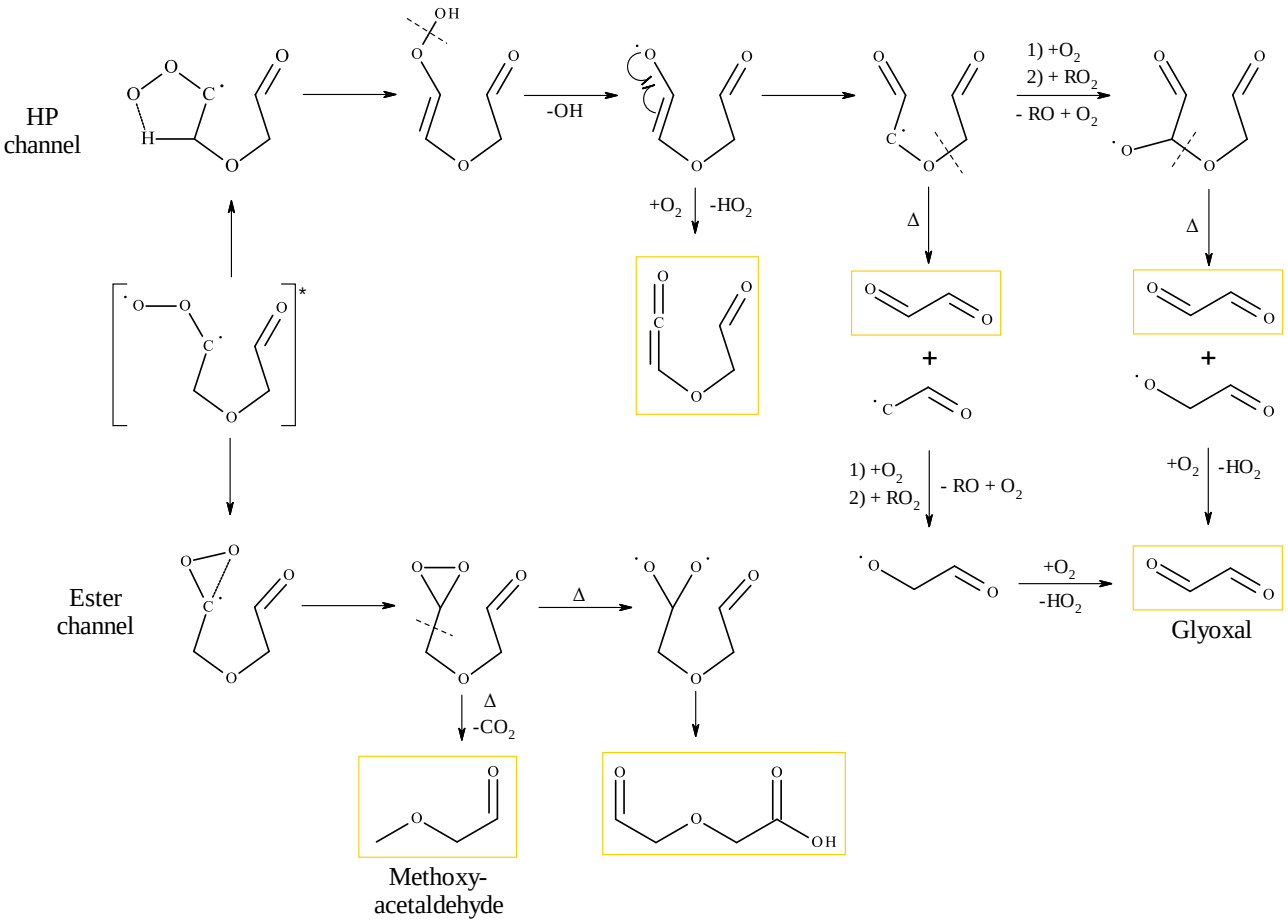

Figure 7.7 Proposed decomposition mechanism of CI of 2,5-DHF.
Potential reaction products following the Hydroperoxy- and Ester-channel,
including Glyoxal and Methoxyacetaldehyde. Stable products are marked in yellow.

HP channel — CI enters the *Hydroperoxide channel* through 1,4H-shift forming a peroxide, as a result it goes from being a biradical to compound comprising a C=C, which in turn may decompose to a vinoxy radical releasing a hydroxyl radical. This channel is estimated to be an important source of hydroxyl radicals in polluted atmosphere (Vereecken & Fransisco, 2012). The vinoxy radical may either react with oxygen, releasing a hydrogen forming $C(O)CHOCH_3CHO$ or it may decompose to form Glyoxal through a set of reactions.

Ester channel — CI enters the *Ester channel* through cyclisation. The product may than either decompose to CO_2 and Methoxyacetaldehyde or through O–O scission finally forming a carboxylic acid, $C(O)HCH_3OCH_3C(O)OH$.

As seen in Figure 7.7 aldehydes, i.e. glyoxal, which is the smallest dialdehyde, and larger carboxylic acids could be formed during the 2,5-DHF ozonolysis. The larger reaction products in Figure 7.7 may belong to the broader peak in 2,5-DHF reaction spectra, Figure 7.2, but could not be confirmed due to the poor resolution of the theoretical vibrational spectra. However, the experimental product study indicated on smaller carbonyl products, such as formaldehyde and formic acid, suggesting that the products formed in Figure 7.7 follow additional decomposition pathways.

The first reaction products in the 2,3-DHF ozonolysis following the *Hydroperoxide*- and *Ester channel* are presented in Figure 7.8.

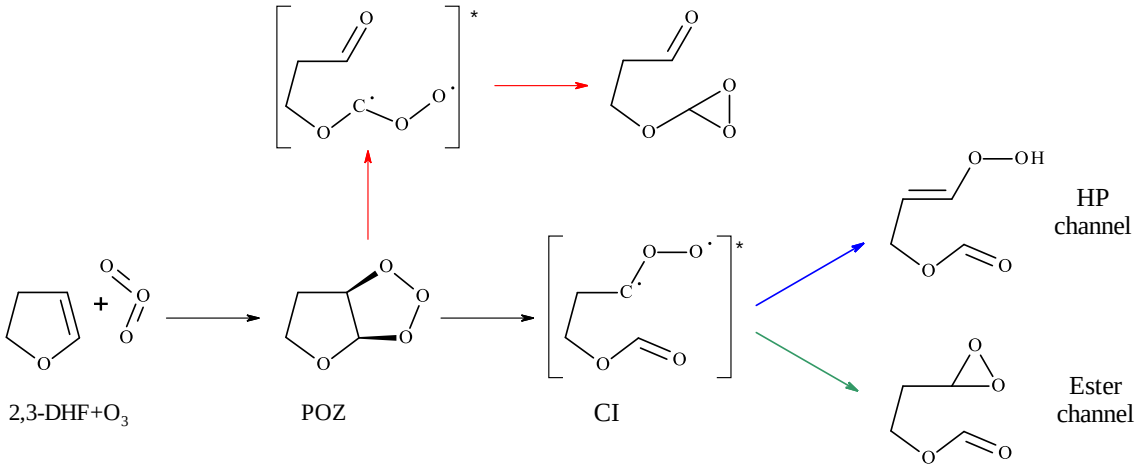

Figure 7.8 Proposed decomposition mechanism of the 2,3-DHF Criegee Intermediate.
The blue, green and red arrow refers to the corresponding transitions states in Figure 7.9.

7.2.1 Potential Energy Surfaces

Chemical computations have been performed in order to distinguish between the difference in the ozonolysis of 2,3- and 2,5-DHF. The result is presented in Table 7.2 and is illustrated as a PES in Figure 7.9. The two DHF are following the same reaction pattern up to the second transition state, TS 2, with 2,3-DHF generally resulting in energies slightly lower than 2,5-DHF. The reaction pattern in Figure 7.9 resembles that of the literature in Figure 5.2. Additionally the result is consistent with the experimental result, that is 2,3-DHF reacts faster with ozone than 2,5-DHF as a result of the larger release energy during the ozonolysis process.

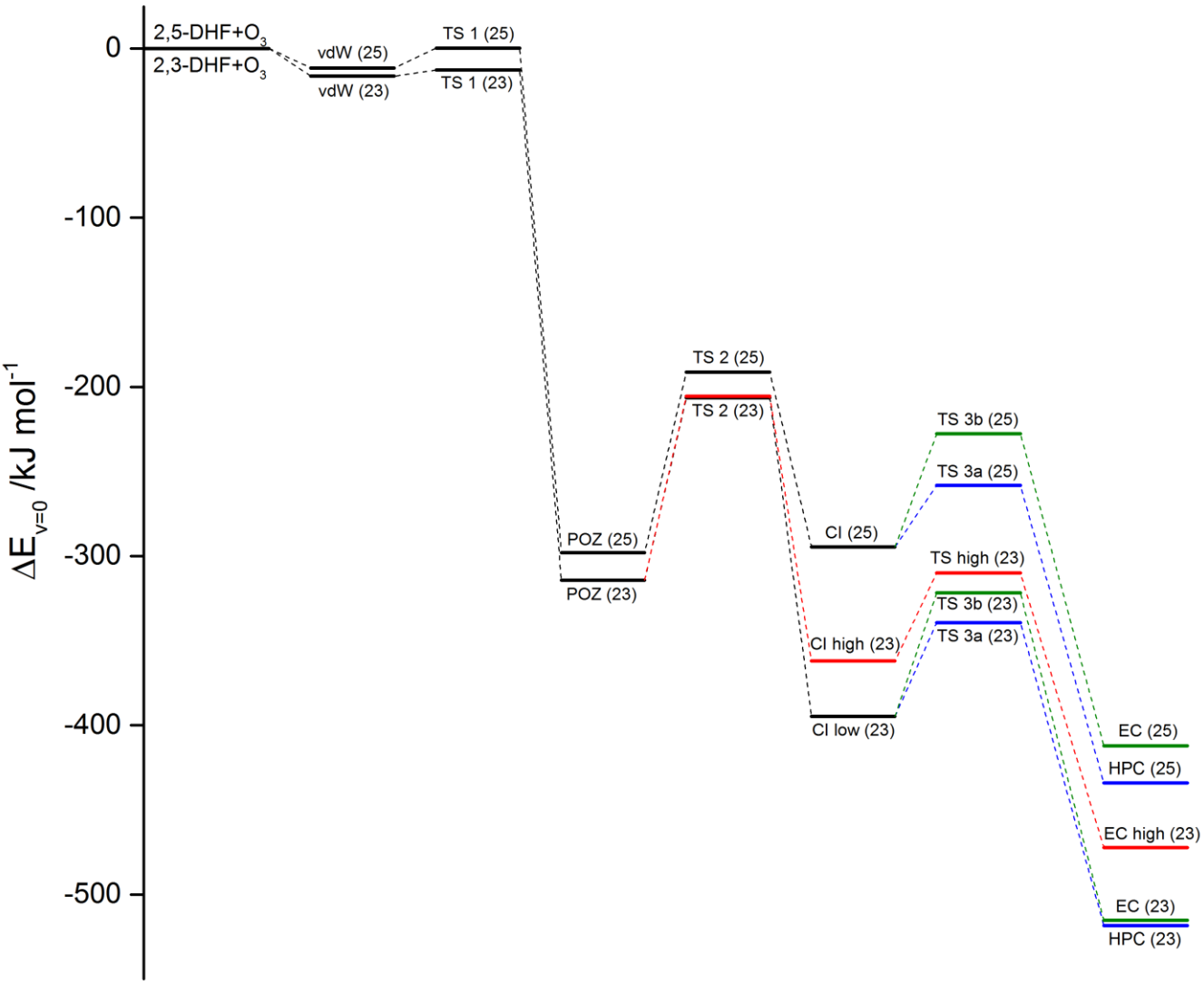

Figure 7.9 *Potential Energy Surface* describing the 2,3- and 2,5-DHF ozonolysis. Numbers within parentheses denotes the 2,3- and 2,5-DHF species.

Ozonolysis is associated highly exothermic reactions as the internal energy released in the POZ formation is ~ 50-60 kcal mol^{-1} (Vereeken & Fransisco, 2012). Ozonolysis of cyclic compounds would therefore release even larger amounts of energy as result of the high internal energy of the initial compound due to ring strain. As a result, the energetic ozonolysis proceed through a set of intermediates, POZ and CI, which are usually undetectable under normal conditions.

After TS 2, during which the POZ splits up into CI, the reaction patterns starts to diverge. CI(2,5-DHF) actually ends up at energies slightly higher than the previous intermediate, POZ(2,5-DHF). It may be due to a computational error, since this data point stands out from the rest following the same reaction pattern. However, it is possible for a reaction intermediate to obtain higher energies than the previous one as long as the final reaction product obtains lower energies than the sum of the reactants energies, see Chapter 5.3.1. Finally, due the small difference in energy between the *Hydroperoxide-* and *Ester channel* both pathways are considered equally probable, HPC(2,5-DHF) ≈ EC(2,5-DHF).

POZ(2,3-DHF) may split in two ways, resulting in two different CI(2,3-DHF), see Figure 7.8. One CI obtains higher internal energy than the other depending on the position of the peroxy radical group. As mentioned above, CI containing higher energy may still be a potential intermediate if the energies of the final reaction products are low enough. In the ozonolysis of 2,3-DHF both CI were evaluated in order to estimate which reaction path is the most probable. For the CI(2,3-DHF) resulting in higher energies only the Ester channel was evaluated since this CI does not contain a hydrogen suitable for a 1,4H-shift into the Hydroperoxyl channel, see Figure 7.8.

In the ozonolysis of 2,3-DHF, both CI results in reaction products with energy lower than the sum of the initial products internal energies, meaning that both reaction paths ways are possible. However, the more energetic CI results in a final reaction product with energies slightly higher than the other two products. Finally the difference in energy between the two decomposition channels is even smaller for 2,3-DHF than for 2,5-DHF and it is therefore likely that both channel products are being formed, HPC(2,5-DHF) ≈ EC(2,5-DHF).

Table 7.2 Energies calculated with M06-2XX/aTZ for the ozonolysis of 2,3-DHF and 2,5-DHF respectively. E_h (Hartree), *ZPE* (Hartree) and ΔE (kJ mol^{-1})/(kcal mol^{-1}).

Species	E_h	*ZPE*	Sum	ΔE (kJ mol^{-1})	ΔE (kcal mol^{-1})
2,3-DHF	-231.2104	0.0939			
O_3	-225.4055	0.0080			
Sum reactants	-456.6159	0.1019	-456.5140	0.0000	0.0000
vdW complex	-456.6237	0.1035	-456.5203	-16.3619	-3.9106
TS 1	-456.6228	0.1039	-456.5189	-12.7027	-3.0360
POZ	-456.7428	0.1091	-456.6337	-314.2040	-75.0967
TS 2a	-456.6978	0.1055	-456.5923	-205.5196	-49.1204
CI high	-456.7561	0.1042	-456.6519	-362.0643	-86.5354
TS high	-456.7354	0.1033	-456.6321	-309.9526	-74.0804
EC high	-456.7991	0.1052	-456.6939	-472.2554	-112.8717
TS 2b	-456.6980	0.1053	-456.5930	-206.5446	-49.3654
CI low	-456.7694	0.1050	-456.6644	-394.8271	-94.3659
TS 3a	-456.7445	0.1013	-456.6432	-339.2636	-81.0860
HPC	-456.8178	0.1064	-456.7116	-518.3571	-123.8903
TS 3b	-456.7399	0.1033	-456.6365	-321.6549	-76.8774
EC	-456.8166	0.1063	-456.7103	-515.3234	-123.1652

Species	E_h	*ZPE*	Sum	ΔE (kJ mol^{-1})	ΔE (kcal mol^{-1})
2,5-DHF	-231.2053	0.0934			
O_3	-225.4055	0.0080			
Sum reactants	-456.6108	0.1014	-456.5094	0.0000	0.0000
vdW complex	-456.6168	0.1030	-456.5138	-11.4894	-2.7460
TS 1	-456.6130	0.1037	-456.5093	0.2707	0.0647
POZ	-456.7319	0.1090	-456.6229	-298.0612	-71.2383
TS 2	-456.6879	0.1057	-456.5822	-191.2598	-45.7122
CI	-456.7250	0.1034	-456.6216	-294.6798	-70.4302
TS 3a	-456.7067	0.0990	-456.6077	-258.1649	-61.7029
HPC	-456.7796	0.1049	-456.6747	-434.0641	-103.7438
TS 3b	-456.6973	0.1012	-456.5961	-227.5881	-54.3949
EC	-456.7755	0.1048	-456.6708	-412.2174	-98.5223

8 Atmospheric Implications

Biofuels are considered to be an environmental friendly alternative to fossil fuels as they have the potential to reduce the global emissions of GHG. Furanic fuels have been proposed as second generation biofuels as they can be produced from crops residues and forest waste. In this work, the atmospheric fate of three furanic compounds, namely furan, 2,3-DHF and 2,5-DHF, was investigated. The results, summarised in Table 8, imply that the furanic compounds will mainly decompose due to tropospheric reaction with OH. The furanic Cl reaction may become important, close to local chlorine sources, in highly polluted urban areas were elevated VOC concentrations result in increased competition for the OH reaction.

As a result of the furanic atmospheric lifetimes, compounds emitted in an already polluted area never manage to leave the region, and will therefore affect the air quality on a local scale. The results of the product study propose that furanic ozonolysis produces shorter oxygenated organic compounds such aldehydes and carboxylic acids. Formaldehyde and formic acid, which could be identified in the reaction spectra, are both common atmospheric compounds. Aldehydes are generally produced in the tropospheric oxidative cycle (A5.6) and are known to elevate tropospheric ozone levels (A5.7-A5.10) (Jacobson, 2007). Furthermore, carboxylic acids may also react with ozone forming additional aldehydes. Consequently, the furanic ozonolysis decomposition products reproduce and could even enhance tropospheric ozone levels causing respiratory problems and increased mortality rates. This study shows that furanic biofuels decompose to atmospheric compounds related to elevated tropospheric ozone levels and urban air pollution. Atmospheric emission of these compounds can therefore be expected to result in elevated levels of tropospheric ozone.

Furanic biofuels are considered to be an environmental friendly solution to the climate change. However, the result of this study indicates that furanic combustion could cause increased regional air pollution with severe local effects. Hence, there is a trade-off between the environmental effects arising from the climate change and air pollution related with furanic combustion. Air pollution is primarily a problem on local and regional scale while climate change is expected to result in environmental problems on a global scale. Furthermore, the effects of air pollution can be expected to act on shorter time scale compared to the long term effects related to climate change. It is difficult to estimate which environmental problems will have largest effect on human health and result in highest mortality rates. The question is:

What tropospheric ozone levels can be considered justified
in order mitigate climate change?

Table 8 Summary of the experimental result of the kinetic study, presenting the reaction rate constants, *k*, and resulting atmospheric lifetime, τ, in polluted and clean air. The result is presented together with literature data for the furanic OH reaction.

	Furan	2,3-DHF	2,5-DHF
k_{O_3}	$2.39 \pm 0.09 \times 10^{-18}$	—	$1.68 \pm 0.07 \times 10^{-17}$
τ (urban)	77.5 h	—	11.0 h
τ (rural)	10 days	—	1.5 days
k_{Cl}	$2.36 \pm 0.11 \times 10^{-10}$	$7.17 \pm 0.75 \times 10^{-10}$	$3.47 \pm 0.17 \times 10^{-10}$
τ (urban/maritime)	11.8 h	3.9 h	8.0 h
τ (rural)	490 days	162 days	334 days
k_{OH}	$4.01 \pm 0.30 \times 10^{-11}$ (1	$1.20 \pm 0.28 \times 10^{-10}$ (2	$6.45 \pm 1.69 \times 10^{-11}$ (2
τ (global)	6.9 h	2.3 h	4.3 h

1) Atkinson et al., 1983.
2) Alwe et al., 2014.

8.1 Conclusions

This project aimed to improve the understanding of the atmospheric impact related to the use of furanic fuels as second generation biofuels. This was done through experimental kinetic- and theoretical mechanistic ozonolysis studies. The result of the laboratory study is presented in Table 8 above together with a discussion regarding the atmospheric implications of furanic combustion. The next section will present the answers to the questions given in Chapter 1.1 followed by an outlook for future work to be done in the field.

8.1.1 Answer to questions

1) How does the rate of saturation affect the atmospheric furanic reactivity?

Furanic compounds become more reactive towards ozone and Cl with increased saturation, e.g. DHF, see Figure 6.4.

2) How does the oxygen position in relation to the double bond affect the atmospheric DHF reactivity?

The oxygen position has major effect on the DHF reactivity towards ozone and Cl. The difference in reactivity against Cl is larger between the two DHF than between 2,5-DHF and furan, indicating that the oxygen position is being more important than the rate of saturation. With the present ozone data it is not possible to estimate if the oxygen position or the rate of saturation has the largest effect on the furanic ozone reactivity.

3) How does the atmospheric furanic reactivity towards Cl differ from its reactivity towards OH?

The furanic Cl reactivity is generally one order of magnitude faster than towards OH. However, the furanic reaction with OH will still dominate as a result of the high OH concentrations in the troposphere.

4) What are the furanic atmospheric lifetimes?

The atmospheric lifetimes are 6.9 h, 2.3 h and 4.3 h for furan, 2,3-DHF and 2,5-DHF respectively with regarding the rapid tropospheric OH-reaction.

5) Which pollutants are related to the atmospheric furanic ozonolysis?

Furanic ozonolysis is associated with short oxygenated hydrocarbons such as aldehydes and carboxylic acids, mainly formaldehyde and formic acid.

8.2 Outlook

This project has followed the work process illustrated in Figure 4.1. Five out of the six executed relative rate experiments resulted in reliable rate constants within the error limits of the previous studies, see Table 6.1 – 6.2. The reaction of 2,3-DHF with Cl needs to be repeated, one experiment for each reference compound used in the present work, in order to confirm the determined rate constant.

Some decomposition products related to the atmospheric furanic ozonolysis were identified and the DHF decomposition mechanism was further studied using computational methods. However, further work needs to be done in order to determine an atmospheric decomposition mechanism for the 2,5-DHF ozonolysis, see Figure 4.1:5.

Proposals for future work involve supplementary laboratory studies, Figure 4.1-2a, using complementary experimental techniques, such as mass spectrometry (MS) to facilitate further product studies. Also additional high resolution reference absorption spectra belonging to the compounds found to be likely reaction products, based on position of peaks belonging to specific functional groups and resemblance of low quality reference spectra, such as Glyoxal, are required. Besides the product identification, these spectra could be used for further product quantifications, Figure 4.1:4b, which are necessary in order to understand the decomposition mechanism.

Additional chemical computation, e.g. branching ratios, may contribute to the understanding of furanic ozonolysis. With calculations of the theoretical reaction rate constants the reliability of the computational method could be validated through comparison with the experimental results.

Once the final atmospheric decomposition mechanism describing the ozonolysis of 2,5-DHF have been established it can be extended to other furanic compounds, such as furan and 2,3-DHF, but also substituted furans, e.g. 2,5-DMF, see Figure 3.2. These atmospheric ozonolysis mechanisms may be implemented in an atmospheric chemical model and further connected to a life cycle analysis (LCA) describing the effects of the furanic fuels.

References

Adeniji, S.A., J.A. Kerr and M.R. Williams (1981) Rate Constants for Ozone-Alkane Reactions Under Atmospheric Conditions *International Journal of Chemical Kinetics* **13**: 209-217 ISSN: 0538-8066

Alecu, I.M., J. Zheng, Y. Zhao and D.G. Truhlar (2010) Computational Thermochemistry: Scale Factor Databases and Scale Factors for Vibrational Frequencies Obtained from Electronic Model Chemistries *Journal of Chemical Theory & Computation* **6**: 2872-2887 DOI: 10.1021/ct100326h

Alwe, H.D., M. Walawalkar, A. Sharma, K.K. Pushpa, S. Dhanya, and P.D. Naik (2013) Rate Coefficients for the Gas-Phase Reactions of Chlorine Atoms with Cyclic Ethers at 298 K *International Journal of Chemical Kinetics* **45**: 295-305 DOI: 10.1002/kin.20765

Alwe, H.D., M.P. Walavalkar, A. Sharma, S. Dhanya and P.D. Naik (2014) Tropospheric Oxidation of Cyclic Unsaturated Ethers in the Day-Time: Comparison of the Reactions with Cl, OH and O_3 Based on the Determination of Their Rate Coefficients at 298 K *Atmospheric Environment* **82**: 113-120 DOI: 10.1002/kin.20765

Andersen, V.F. (2012) Physical Properties and Atmospheric Chemistry of Biofuels – PhD thesis *University of Copenhagen: Department of Chemistry* Copenhagen, Denmark

Andersen, V.F., K.B. Ørnsø, S. Jørgensen, O.J. Nielsen and M.S. Johnson (2012) Atmospheric Chemistry of Ethyl Propionate *Journal of Physical Chemistry* **116**: 5164-5179 DOI: dx.doi.org/10.1021/jp300897t

Aschmann, S.M., A.A. Chew, J. Arey and R. Atkinson (1997) Products of the Gas-Phase Reaction of OH Radicals with Cyclohexane: Reactions of the Cyclohexoxy Radical *Journal Physical Chemistry A* **101**: 8042-8048 DOI: 10.1021/jp971869f

Atkins, P. and J. de Paula (2010) Atkins' Physical Chemistry – 9th ed. *Oxford University Press Inc.* New York, United States of America ISBN: 9780199583973

Atkinson, R., S.M. Aschmann, W.P.L. Carter and J.N. Pitts Jr. (1983a) Effects of Ring Strain on Gas-Phase Rate Constants. I. Ozone Reactions with Cycloalkanes *International Journal of Chemical Kinetics* **15**: 721-731 DOI: 10.1002/kin.550150804

Atkinson, R., S.M. Aschmann and W.P.L. Carter (1983b) Kinetics of the Reactions of O_3 and OH Radicals with Furan and Thiophene at 298 ± 2 K *International Journal of Chemical Kinetics* **15**: 51-61 DOI: 10.1002/kin.550150106

Atkinson R., D.L. Baulch, R.A. Cox, J.N. Crowley, R.F. Hampson, R.G. Hynes, M.E. Jenkin, M.J. Rossi et al. (2004) IUPAC Task Group on Atmospheric Chemical Kinetic Data Evaluation *Atmospheric Chemistry and Physics* **4**: 1461-1738
Available: http://iupac.pole-ether.fr. Vol 2 (June 22, 2015)

Banwell, C.N. and E.M. McCash (1994) Fundamentals of Molecular Spectroscopy – 4th edition *McGraw-Hill Publishing Company* London, United Kingdom ISBN: 978-0-077-07976-5

Cabañas, B., F Villanueva, P. Martin, M. Baeza, S. Salgado and E. Jimenez (2005) Study of Reaction Processes of Furan and Some Furan Derivatives Initiated by Cl atoms *Atmospheric Environment* **39**: 1935-1944 DOI: 10.1016/j.atmosenv.2004.12.013

Chang, S. and D.T. Allen (2006) Atmospheric Chemistry in Southeast Texas: Impacts on Ozone Formation and Control *Environmental Science & Technology* **40**: 251-262 DOI: 10.1021/es050787z

D'Anna, B., A Wisthaler, O Andreasen, A. Hansel, J. Hjorth, N.R. Jensen, C.J. Nielsen, Y. Stenstrom, et al. (2005) Atmospheric Chemistry of C3−C6 Cycloalkanecarbaldehydes *Journal of Physical Chemistry A* **109**: 5104-5118 DOI: 10.1021/jp044495g

EEA (2014) Air pollution fact sheet 2014 – Sweden *European Environmental Agency* Copenhagen, Denmark, 20 pp Available: http://www.eea.europa.eu/themes/air/air-pollution-country-fact-sheets-2014/sweden-air-pollutant-emissions-country-factsheet/view (May 27, 2015)

Engel, T. (2013) Quantum Chemistry and Spectroscopy – 3rd edition *Pearson Education, Inc.* Glenview, United States of America ISBN: 9780321781611

EUROCHAMP (n.d.) *IR Spectral database* [Online] Available: http://euphore.es/FTIRReferences2/index.php (August 17, 2015)

Fang, Y., V. Naik, L.W. Horowitz and D.L. Mauzerall (2013) Air Pollution and Associated Human Mortality: the Role of Air Pollutant Emissions, Climate Change and Methane Concentration Increases From the Preindustrial Period to Present *Atmospheric Chemistry and Physics* **13**: 1377-1394 DOI: 10.5194/acp-13-1377-2013

Foresman, J.B. and Æ. Frisch (1996) Exploring Chemistry with Electronic Structure Methods – 2nd edition *Gaussian Inc.* Pittsburgh, United States of America ISBN: 0-9636769-3-8

Graham, E.L. (2013) Furan: A Future Fuel and its Lifetime in Urban Air - BSc Thesis *Lund University: Combustion Physics* Lund, Sweden Available: http://www.lu.se/lup/publication/3879044 (January 29, 2015)

Griffith, D.W.T. (1996) Synthetic Calibration and Quantitative Analysis of Gas-phase FT-IR spectra *Applied Spectroscopy* **50**: 59-70 DOI: 10.1366/0003702963906627

Gross, A. and S. Jørgensen (2008) Theoretical Determinations of Reaction Parameters for Atmospheric Chemical Reactions - Simulation and Assessment of Chemical Processes in a Multiphase Environment *NATO Science for Peace and Security Series C - Environmental Security* pp. 31-46 DOI: 10.1007/978-1-4020-8846-9_3

Harrison, R.M (1990) Pollution: Causes, Effects and Control *Royal Society of Chemistry* ISBN: 9780851862835

Jacobson, M.Z. (2007) Effects of Ethanol (E85) Versus Gasoline Vehicles on Cancer and Mortality in the United States *Environmental Science & Technology* **41**: 4150-4157 DOI: 10.1021/es062085v

Johnson, D. and G. Marston (2008) The Gas-Phase Ozonolysis of Unsaturated Volatile Organic Compounds in the Troposphere *Chemical Society Reviews* **37**: 699-716 DOI: 10.1039/b704260b

Kasper, T., A. Lucassen, A.W. Jasper, W. Li, P.R Westmoreland, K. Kohse-Höinghaus, B. Yang, J. Wang, T. Cool and N. Hansen (2011) Identification of Tetrahydrofuran Reaction Pathways in Premixed Flames Phys. *Zeitschrift für Physikalische Chemie* **225**: 1237-1270 DOI: 10.1524/zpch.2011.0163

Klumpp, A., W. Ansel, G. Klumpp, V. Calatayud, J.P. Garrec, S. He, J. Peñuelas, À. Ribaset, et al. (2006) Ozone Pollution and Ozone Biomonitoring in European Cities. Part I: Ozone Concentrations and Cumulative Exposure Indices at Urban and Suburban Sites *Atmospheric Environment* **40**: 7963-7974 DOI: 10.1016/j.atmosenv.2006.07.017

Kohse-Höinghaus, K., P. Osswald, T.A. Cool, T. Kasper, N. Hansen, F. Qi, C.K Westbrook, and P.R. Westmoreland, P. R. (2010) Biofuel Combustion Chemistry: from Ethanol to Biodiesel *Angewandte Chemie International Edition* **49**: 3572-3597 DOI: 10.1002/anie.200905335

Lawrence, J.E. and P. Koutrakis (1994) Measurement of Atmospheric Formic and Acetic Acids: Methods Evaluation and Results from Field Studies *Environmental Science and Technology* **28**: 957-964 DOI: 10.1021/es00054a031

Manion J.A., R.E. Huie, R.D. Levin, D.R. Burgess Jr., V.L. Orkin, W. Tsang, W.S. McGivern, J.W. Hudgens, et al. (2013) NIST Chemical Kinetics Database, NIST Standard Reference Database 17, Version 7.0 (Web Version), Release 1.6.8, Data version 2013.03, *National Institute of Standards and Technology*, Gaithersburg, Maryland, 20899-8320.
Available: http://kinetics.nist.gov/ (June 22, 2015)

McMurry, J. (2011) Fundamentals of Organic Chemistry – 7th ed. *Brooks/Cole, Cengage Learning* Belmont, United States of America ISBN: 9781439049730

Monks, P.S. (2005) Gas-phase Radical Chemistry in the Troposphere *Chemical Society Reviews* **34**: 376-395 DOI: 10.1039/b307982c

Naik, S.N., V.V. Goud, P.K. Rout and A.K. Dalai (2010) Production of First and Second Generation Biofuels: A Comprehensive Review *Renewable and Sustainable Energy Reviews* **14**: 578-597 DOI:10.1016/j.rser.2009.10.003

Nilsson, E.J.K., C. Eskebjerg and M.S. Johnson (2009a) A Photochemical Reactor for Studies of Atmospheric Chemistry *Atmospheric Environment* 43 3029-3033 DOI: 10.1016/j.atmosenv.2009.02.034

Nilsson, E.J.K., O.J. Nielsen, M.S. Johnson, M.D. Hurley and T.J. Wallington (2009b) Atmospheric Chemistry of *cis*-$CF_3CH{=}CHF$: Kinetics of Reactions with OH radicals and O_3 and Products of OH Initiated Oxidation *Chemical Physics Letter* **473**: 233-237 DOI: 10.1016/j.cplett.2009.03.076

Rothman, L.S., I.E. Gordon, A. Barbe, D.C. Benner, P.E. Bernath, M. Birk, V. Boudon, V. Brown et al. (2009) The HITRAN 2008 molecular spectroscopic database *Journal of Quantitative Spectroscopy and Radiative Transfer* **110**: 533-572 DOI: 10.1016/j.jqsrt.2009.02.013

Scovronick, N and P. Wilkinson (2014) Health Impacts of Liquid Biofuel Production and Use: a Review *Global Environmental Change* **24**: 155-164 DOI: 10.1016/j.gloenvcha.2013.09.011

Seinfeld, J.H. and S.N. Pandis (2006) Atmospheric Chemistry and Physics: from Air Pollution to Climate Change – 2nd ed. *John Wiley & Sons* New Jersey, United States of America ISBN: 9780471720188

Sharma A., K.K. Pushpa, S. Dhanya, P.D. Naik and P.N. Bajaj (2010) Rate Coefficients and Products for Gas-Phase Reactions of Chlorine Atoms with Cyclic Unsaturated Hydrocarbons at 298 K *International Journal of Chemical Kinetics* **42**: 98-105 DOI: 10.1002/kin.20467

Sirignano, M., M. Conturso and A. D'Anna (2015) Effect of Furans on Particle Formation in Diffusion Flames: an Experimental and Modeling Study *Proceedings of the Combustion Institute* **35**: 525–532 DOI:10.1016/j.proci.2014.05.062

Sy Tran, L., B. Sirjean, P.A. Glaude, R. Fournet and F. Battin-Leclerc (2012) Progress in Detailed Kinetic Modeling of the Combustion of Oxygenated Components of Biofuels *Energy* **43**: 4-18 DOI: 10.1016/j.energy.2011.11.013

Toby, S., L.J. Van de Burgt and F.S. Toby (1985) Kinetics an Chemiluminescence of Ozone-Aromatic Reactions in the Gas Phase *Journal of Physical Chemistry* **89**: 1982-1986 DOI: 10.1021/j100256a034

Uherek, E., T. Halenka, J. Borken-Kleefeld, Y. Balkanski, T. Berntsen, C. Borrego, M. Gauss, P. Hoora, et al. (2010) Transport Impacts on Atmosphere and Climate: Land Transport. *Atmospheric environment* **4**: 4772–4816 DOI: 10.1016/j.atmosenv.2010.01.002

vanLoon, G.W. and S.J. Duffy (2011) Environmental Chemistry: a Global Perspective – 3rd ed. *Oxford University Press Inc.* New York, United States of America ISBN: 9780199228867

Vereecken L. and J.S. Fransisco (2012) Theoretical Studies of Atmospheric Reaction Mechanisms in the Troposphere *Chemical Society Reviews* **41**: 6259-6293 DOI: 10.1039/c2cs35070j

Voll, A. and W. Marquardt (2012) Benchmarking of Next-Generation Biofuels From a Process Perspective *Biofuels, Bioproducts & Biorefining* **6**: 292-301 DOI: 10.1002/bbb.1325

Williams, D.H. and I. Fleming (1995) Spectroscopic Methods in Organic Chemistry – 5th ed. *McGraw-Hill Higher Education* Berkshire, United Kingdom ISBN: 0077091477

Young, C.J., R.A. Washenfelder, P.M. Edwards, D.D. Parrish, J.B. Gilman, W.C. Kuster, L.H. Mielke, H.D. Osthoff, et al. (2014) Chlorine as a Primary Radical: Evaluation of Methods to Understand its Role in Initiation of Oxidative Cycles *Atmospheric Chemistry and Physics* **14**: 3427-3440 DOI: 10.5194/acp-14-3427-2014

Zheng, J., I. M. Alecu, B. J. Lynch, Y. Zhao and D. G. Truhlar *Database of Frequency Scale Factors for Electronic Model Chemistries* (Online)
Available: http://t1.chem.umn.edu/freqscale/index.html (January 30, 2015)

Appendix A – Atmospheric Chemistry

The following appendix summarizes some of the atmospheric chemical reactions that the prior report is based on. If nothing else is stated, the chemistry presented in this section is obtained from Atmospheric Chemistry and Physics *by Seinfeld and Pandis (2006).*

A1 Chapman Mechanism

Atmospheric ozone production is highly correlated with the surrounding oxygen atom concentrations. In the presence of a third stable body (M) the oxygen atom is able to react with O_2 resulting in O_3 (A1.2), which is the only reaction through which atmospheric ozone is being produced. Free oxygen atoms can be produced in two different ways in the atmosphere; through short wave photo dissociation of oxygen molecules or is released through different tropospheric chemical reactions, described later in this appendix. At altitudes higher than 30 km, the solar radiation is energetic enough to split O_2, causing the stratosphere to be the largest source of atmospheric of ozone.

$$O_2 + h\nu \rightarrow O + O \qquad (< 242\ \text{nm}) \qquad \text{A1.1}$$

$$O + O_2 \xrightarrow{M} O_3 \qquad \text{A1.2}$$

Stratospheric ozone is decomposed back into O_2 and an oxygen atom through photo dissociation at two different wavelengths bands:

$$O_3 + h\nu \rightarrow O_2 + O \qquad (400 - 600\ \text{nm}) \qquad \text{A1.3a}$$

$$\rightarrow O_2 + O(^1D) \qquad (< 320\ \text{nm}) \qquad \text{A1.3b}$$

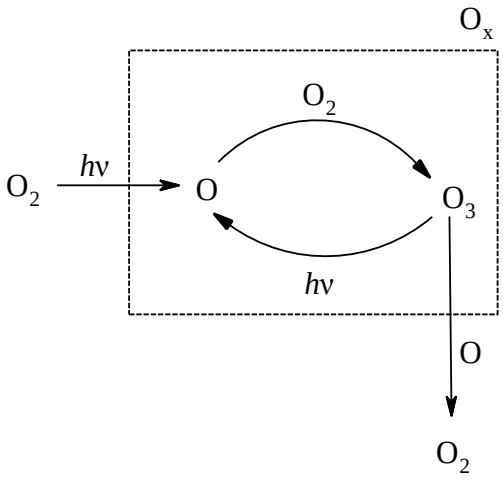

Figure A1. The Chapman cycle.
(Derived from the stratospheric ozone chemistry presented in Seinfeld & Pandis, 2006)

Reaction A1.3b results in an excited oxygen atom, $O(^1D)$, that is rapidly being quenched back into its ground state through collision with a third body, M:

$$O(^1D) \xrightarrow{M} O$$

Reaction A1.1-A1.3 is generally referred to as the Chapman cycle, illustrated in Figure A1, a catalytic cycle that is terminated through the reaction of ozone with a free oxygen atom:

$$O + O_3 \rightarrow 2O_2 \qquad \text{A1.4}$$

A2 NO_x cycle

The NO_x cycle, Figure A2, is initiated by the photo dissociation of nitrous oxide, N_2O, releasing a free oxygen atom that can split remaining N_2O into either two nitric oxide molecules, NO, or nitrogen and oxygen:

$$N_2O + h\nu \rightarrow N_2 + O(^1D) \qquad \text{A2.1}$$

$$N_2O + O(^1D) \rightarrow NO + NO \qquad \text{A2.2a}$$
$$\rightarrow N_2 + O_2 \qquad \text{A2.2b}$$

Nitric oxide reacts with ozone producing nitrogen dioxide, NO_2, which in turn reacts with a free oxygen atom in order to reproduce nitric oxide:

$$NO + O_3 \rightarrow NO_2 + O_2 \qquad \text{A2.3}$$
$$NO_2 + O \rightarrow NO + O_2 \qquad \text{A2.4}$$

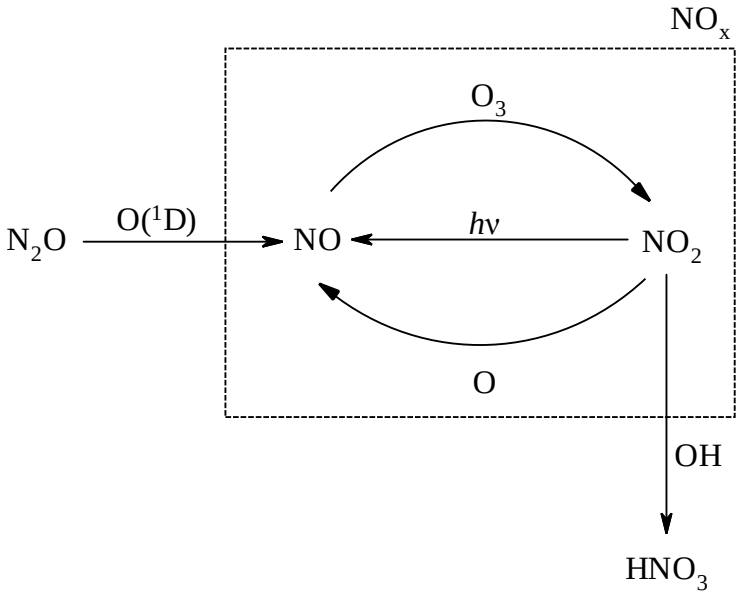

Figure A3. The NO_x cycle.
(Derived from the tropospheric chemistry presented in Seinfeld & Pandis, 2006)

Nitrogen dioxide may be further dissociated by photolysis:

$$NO_2 + h\nu \rightarrow NO + O \qquad (\lambda < 420\ \text{nm}) \qquad \text{A2.5}$$

Photolysis of NO_2 followed by A1.2 is the only known mechanism for ozone production to occur in the troposphere. The NO_x cycle is finally terminated by the deposition of NO_2 and OH through nitric acid, HNO_3:

$$NO_2 + OH \xrightarrow{M} HNO_3 \qquad \text{A2.6}$$

A3 HO_x cycle

The hydroxyl radical, OH, is a secondary product of ozone photo dissociation at wavelengths shorter than 320 nm (A1.3b). The collision of the excited oxygen atom with H_2O is the only atmospheric reaction energetic enough in order to break the O-H bond in a water molecule producing the hydroxyl radical. Tropospheric OH concentrations are generally higher in the southern hemisphere as result of the larger water bodies and lower number of pollutants.

In the stratosphere water concentrations rarely exceeds 5-6 ppm due to the efficient freezing out of water in rising air parcels passing the extremely cold tropopause. Instead stratospheric hydroxyl radical is produced in the oxidation methane, which is highly reactive towards $O(^1D)$:

$$H_2O + O(^1D) \rightarrow 2OH \qquad \text{A3.1a}$$
$$CH_4 + O(^1D) \rightarrow CH_3^{\bullet} + OH \qquad \text{A3.1b}$$

$$OH + O_3 \rightarrow HO_2 + O_2 \qquad \text{A3.2}$$

As the hydroperoxyl radical, HO_2, is decomposed in set of different reactions the hydroxyl radical is regenerated in the catalytic cycle, Figure A3:

$$HO_2 + NO \rightarrow NO_2 + OH \qquad \text{A3.3}$$

$$HO_2 + O \rightarrow O_2 + OH \qquad \text{A3.4a}$$
$$HO_2 + O_3 \rightarrow 2O_2 + OH \qquad \text{A3.4b}$$

The HO_x cycle is finally terminated through (A2.6), producing nitric acid or through the reaction of hydroperoxyl radical with atmospheric chlorine:

$$HO_2 + ClO \rightarrow O_2 + HOCl \qquad \text{A3.5}$$

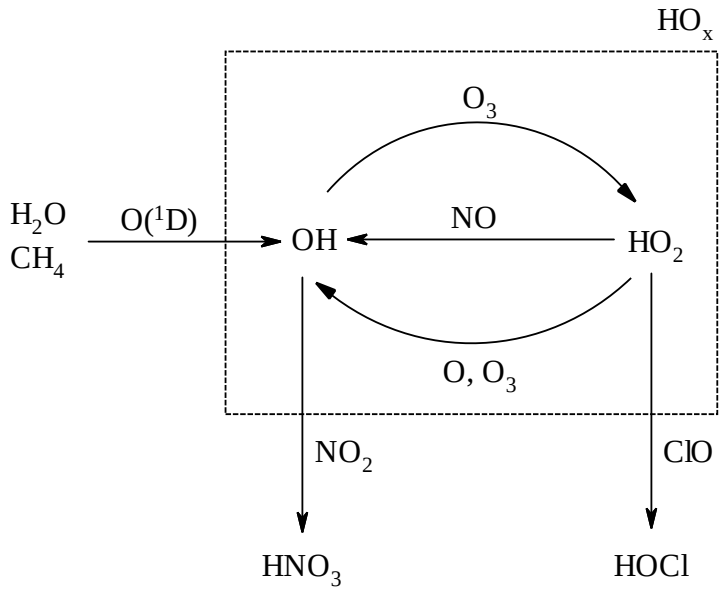

Figure A3. The HO_x cycle.
(Derived from the tropospheric chemistry presented in Seinfeld & Pandis, 2006)

The hydroxyl radical is considered the detergent of the troposphere as it is highly reactive towards VOC, while in clean air the main reaction pathway is via carbon monoxide:

$$CO + OH \rightarrow CO_2 + H \qquad \text{A3.6}$$

$$H + O_2 \xrightarrow{M} HO_2 \qquad \text{A3.7}$$

For the more polluted mechanism, see the tropospheric chemistry section below.

A4 ClO_x cycle

Chlorine is the most abundant halogen in the atmosphere, it enter the troposphere via chlorinated compounds emitted by industrial processes and the ocean as sea spray aerosols and gaseous halocarbons. Free chloride radicals are formed through photo dissociation of these compounds, for example nitryl chloride, $ClNO_2$ (Young et al., 2014):

$$ClNO_2 + h\nu \rightarrow Cl + NO_2 \qquad \text{A4.1}$$

The chlorine radical is highly reactive towards ozone, a reaction which rapidly produces chlorine monoxide:

$$Cl + O_3 \rightarrow ClO + O_2 \qquad \text{A4.2}$$

which may serve as an ozone sink. Chlorine monoxide regenerates the free chlorine radical through reaction with molecular oxygen or nitric oxide, resulting in the catalytic ClO_x cycle:

$$ClO + O \rightarrow Cl + O_2 \quad \text{A4.3}$$

$$ClO + NO \rightarrow Cl + NO_2 \quad \text{A4.4a}$$

$$ClO + NO \rightarrow ClNO_2 \quad \text{A4.4b}$$

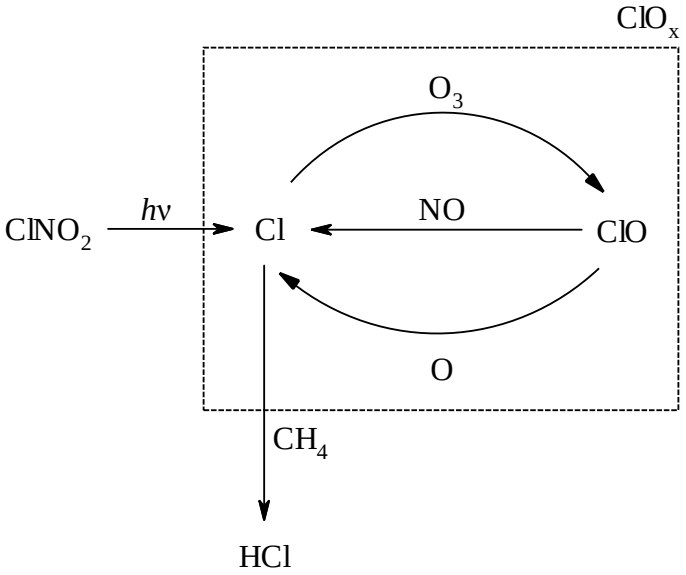

Figure A4. The ClO_x cycle.
(Derived from the tropospheric chemistry presented in Seinfeld & Pandis, 2006)

The ClO_x cycle may be terminated by chlorine reaction with methane:

$$Cl + CH_4 \rightarrow CH_3^{\bullet} + HCl \quad \text{A4.5}$$

or ClO being oxidized through reaction with hydroperoxyl radical (A3.5) or the hydroxyl radical:

$$Cl + OH \rightarrow HOCl \quad \text{A4.6}$$

A5 Tropospheric Chemistry

Once released into the atmosphere VOC enters the tropospheric oxidative cycle presented in Figure A5. This tropospheric VOC oxidation is initiated by reaction with the hydroxyl radical, A5.1a or a free chlorine radical:

$$OH + RH \rightarrow H_2O + R^{\bullet} \quad \text{A5.1a}$$

$$Cl + RH \rightarrow HCl + R^{\bullet} \quad \text{A5.1b}$$

followed by several oxidative processes, A5.2 – A5.5:

$$R^{\bullet} + O_2 \xrightarrow{M} RO_2^{\bullet} \quad \text{A5.2}$$

$$RO_2^{\bullet} + NO \xrightarrow{M} RONO_2 \qquad \text{A5.3a}$$

$$RO_2^{\bullet} + NO \rightarrow RO^{\bullet} + NO_2 \qquad \text{A5.3b}$$

$$RO_2^{\bullet} + RO_2^{\bullet} \rightarrow 2RO^{\bullet} + O_2 \qquad \text{A5.4}$$

Under clean conditions the peroxy radical may react as follows:

$$RO_2^{\bullet} + HO_2 \rightarrow ROOH + O_2 \qquad \text{A5.5}$$

Finally a hydroperoxide radical and a carbonyl is obtained

$$RO^{\bullet} + O_2 \rightarrow R(O)H + HO_2 \qquad \text{A5.6}$$

The carbonyl may be further decomposed, forming additional pollutants, while the hydroperoxide radical is reduced through reaction with NO (A3.3) to a hydroxyl radical able to restart the process, see the area marked in blue in Figure A5.

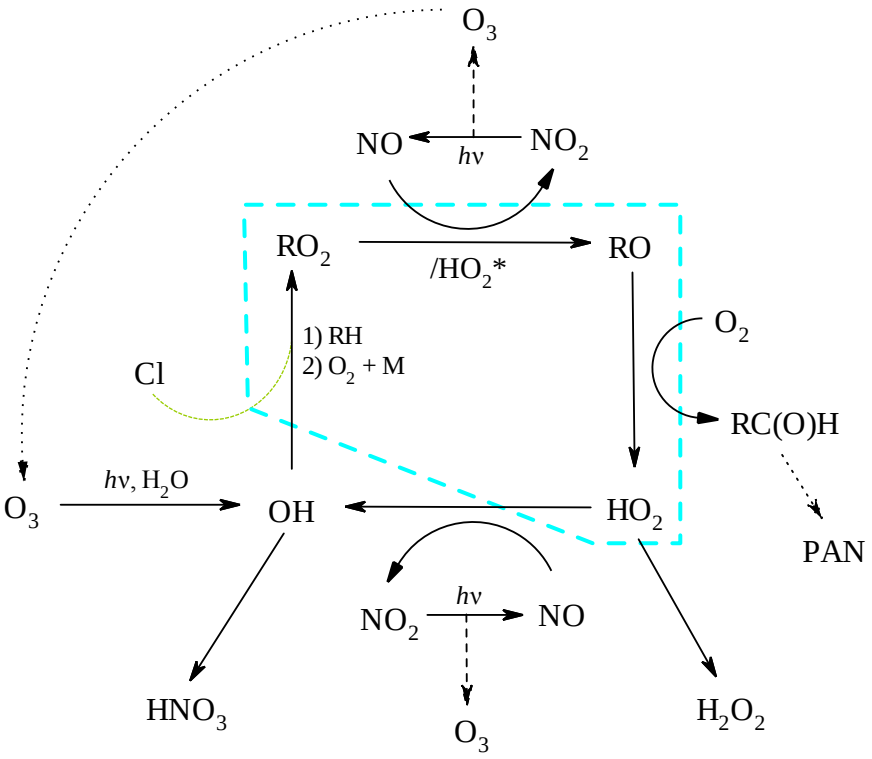

Figure A5. Generalized mechanism of the tropospheric chemical reactions.
The area marked in blue denotes the VOC oxidation.
*Reaction with HO_2 takes part under clean conditions.
(Derived from the tropospheric chemistry presented in Seinfeld & Pandis, 2006)

Aldehydes, emitted to or formed in the troposphere, undergo photolysis or chemical reaction with NO_3 or hydroxyl radicals involving H-abstraction forming an acyl radical:

$$RC(O)H + OH \rightarrow RC^{\bullet}O + H_2O \qquad A5.7$$

which rapidly reacts with oxygen:

$$RC^{\bullet}O + O_2 \xrightarrow{M} RC(O)OO^{\bullet} \qquad A5.8$$

The resulting acyl peroxy radical reacts with NO_x:

$$RC(O)OO^{\bullet} + NO \rightarrow RC(O)O^{\bullet} + NO_2 \qquad A5.9$$

$$RC(O)O^{\bullet} \rightarrow R^{\bullet} + CO_2 \qquad A5.10$$

were $R^{\bullet}$ enters the tropospheric oxidative cycle via A5.2.

$$RC(O)OO^{\bullet} + NO_2 \overset{M}{\rightleftarrows} RC(O)OONO_2 \qquad A5.11$$

known as the toxic peroxyacyl nitrates (PAN).

A6 Nocturnal Chemistry

At night the NO_x slow down due to the absence of sunlight, remaining NO reacts with O_3 resulting in NO_2 (A2.3), which take part of the nocturnal ozone destruction:

$$NO_2 + O_3 \rightarrow NO_3 + O_2 \qquad A6.1$$

producing nitrate radicals, NO_3, also reactive towards NO_2:

$$NO_3 + NO_2 \xrightarrow{M} N_2O_5 \qquad A6.2$$

Although N_2O_5 usually thermally decompose back:

$$N_2O_3 \xrightarrow{M} NO_3 + NO_2 \qquad A6.3$$

resulting in an equilibrium on a time scale of a few minutes. N_2O_5 may also be terminated through the heterogeneous (particle-phase) hydrolysis:

$$N_2O_5 + H_2O(s) \rightarrow 2HNO_3 \qquad A6.4$$

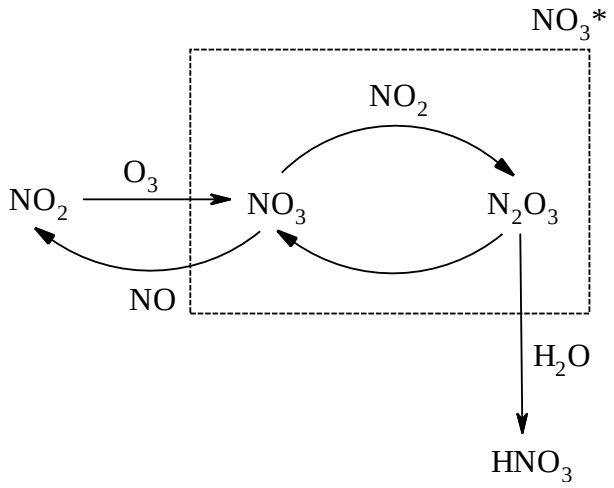

Figure A7. The NO_3*-cycle.
(Derived from the tropospheric chemistry presented in Seinfeld & Pandis, 2006)

If any NO remains after NO3 has been produced the two molecules reacts instantaneously as the two molecules are not able to coexist:

$$NO_3 + NO \rightarrow 2NO_2 \qquad \text{A6.5}$$

In the morning NO_3 is rapidly photolysed back into the NO_x cycle:

$$NO_3 + h\nu \rightarrow NO + O_2 \quad (< 700\ \text{nm}) \qquad \text{A6.6a}$$
$$\rightarrow NO_2 + O \quad (< 580\ \text{nm}) \qquad \text{A6.6b}$$

Appendix B – Previous Work

This appendix summarizes all previously determined rate constants treated in this report.

Table B1. Rate constants in previous ozone experiments.

O_3	k_{O3} ($cm^3\,molec^{-1}\,s^{-1}$)	Conc. (molec cm^{-3})	
Furan	$2.42 \pm 0.28 \times 10^{-18}$ [a]	[Furan] =	$0.367\text{-}1.959 \times 10^{-15}$
		$[O_3]$ =	$1.67\text{-}2.67 \times 10^{-13}$
	$2.24 \pm 0.37 \times 10^{-18}$ [b]	[Furan] =	1 ppm
		$[C_6H_{12}]$ =	10 ppm
		$[O_3]$ =	4-100 ppm
	$(2.51 \pm 0.30 \times 10^{-18})$ [b]		
2,3-DHF	$4432 \pm 790 \times 10^{-18}$ [c]	[2,3-DHF] =	2×10^{-15}
		[THF*] =	$1020\text{-}1242 \times 10^{-15}$
2,5-DHF	$16.5 \pm 3.1 \times 10^{-18}$ [c]	[2,5-DHF] =	$3\text{-}10 \times 10^{-15}$
		[THF*] =	$49\text{-}1254 \times 10^{-15}$
	$46.4 \pm 14.5 \times 10^{-18}$ [b]	[2,5-DHF] =	1 ppm
		$[C_6H_{12}]$ =	10 ppm
		$[O_3]$ =	2-13 ppm
	16.1×10^{-18} [d]	[2,5-DHF] =	Excess
		$[O_3]$ =	0.01-2 ppm

[a] Atkinson, 1983b. 298 ± 2 K and 735 torr. (Including ozone loss without any reactants)

[b] Graham, 2013. 298 ± 2 K and 750 ± 10 torr.

[c] Alwe et al., 2014. 298 ± 2 K and 800 ± 3 torr.

[d] Adeniji, 1981. 294 ± 2 K and 1 atm.

Table B2. Rate constants in previous chlorine experiments.

Cl	k_{Cl} (cm^3 $molec^{-1}$ s^{-1})	Conc. (molec cm^{-3})	
Furan	$2.0 \pm 0.2 \times 10^{-10}$ [a]	[Furan] = [ref] = [$Cl^{\bullet}$ source] =	3-13 ppm 5-18 ppm 32-80 ppm
2,3-DHF	$4.52 \pm 0.99 \times 10^{-10}$ [b]	[2,3-DHF] = [ref] =	200-250 ppm 200-300 ppm
2,5-DHF	$4.48 \pm 0.59 \times 10^{-10}$ [b]	[2,5-DHF] = [ref] =	200-250 ppm 200-300 ppm

[a] Cabañas et al., 2005. 298 ± 2 K and 1 atm.

[b] Alwe et al., 2013. 298 ± 2 K and 800 ± 3 torr.

Table B3. Rate constants in previous OH experiments.

OH	k_{OH} (cm^3 $molec^{-1}$ s^{-1})	Conc. (molec cm^{-3})	
Furan	$40.1 \pm 3.0 \times 10^{-12}$ [a]	[Furan/ref] = [CH_3ONO] = [NO] =	~1 ppm 3-6 ppm ~5 ppm
2,3-DHF	$6.45 \pm 1.69 \times 10^{-11}$ [b]	[2,3-DHF] = [H_2O_2] =	$1\text{-}2 \times 10^{-15}$ $30\text{-}48 \times 10^{-15}$
2,5-DHF	$11.95 \pm 2.79 \times 10^{-11}$ [b]	[25-DHF] = [H_2O_2] =	$0.5\text{-}1 \times 10^{-15}$ $33\text{-}48 \times 10^{-15}$

[a] Atkinson, 1983. 298 ± 2 K and 735 torr. (Including ozone loss without any reactants)

[b] Alwe et al., 2014. 298 ± 2 K and 800 ± 3 torr.

Table B4. Rate constants for the reference compounds used in the project. Rate constants with no specified errors are assumed to include a 3 % error. (Atkinson et al., 2004; Manion et al., 2013, Sharma et al., 2010)

	k_{O3} (cm^3 $molec^{-1}$ s^{-1})	k_{Cl} (cm^3 $molec^{-1}$ s^{-1})
C_2H_4	1.70×10^{-18}	
C_3H_6		2.68×10^{-10}
C_3H_8		1.40×10^{-10}
iso-C_4H_8	1.08×10^{-17} (Manion)	
cyclo-C_7H_{12}		$5.12 \pm 0.55 \times 10^{-10}$ (Sharma)

Appendix C – List of Studied Reference Spectra

Product	Func. Group	Source	Furan	2,3-DHF	2,5-DHF
1-Butene	Alkene	KU	NO	NO	NO
2(5H)furanone	Furanone	KU	**CLOSE**	NO	NO
2-MTHF	Furan	KU			
2,5-DMTHF	Furan	KU	NO	NO	NO
3-Me-2(5H)furanone	Furanone	KU	NO	NO	NO
γ-Valerolactone	Laktone	KU	NO	NO	NO
Acetaladehyde	Aldehyde	KU	NO	NO	NO
Acetic acid	Carboxylic Acid	NIST	NO	NO (close)	NO
Acetylene	Alkyne	KU	NO	NO	NO
Akrolein	Aldehyde	NIST	NO	NO	NO
Butanal	Aldehyde	KU	NO	NO	NO
Butyric Acid	Carboxylic Acid	NIST	NO	NO	NO
Ethene	Olefine	KU	NO	NO	NO
C2H5OC2H5		KU	NO	NO	NO
C2H5OHO		KU	NO	**CLOSE**	NO
Ethane	Alkane	KU	NO	NO	NO
Propene	Alkene	KU	NO	NO	NO
Propane	Alkane	KU	NO	NO	NO
C_5H_{12}		KU	NO	NO	NO
CH3CH2OCH3		KU	NO	NO	NO
CH3CHO		KU	NO	NO	NO

Product	Func. Group	Reference	Furan	2,3-DHF	2,5-DHF
CH3OC(O)CH3		KU	NO	NO	NO
CH3OCHO		KU	NO	NO	NO
DME	Ether	NIST	NO	NO	NO
Etanol	Alcohol	NIST	NO	NO	NO
Ethyl acetate	Ester	KU	NO	NO	NO
Ethyl formate	Ester	NIST	NO	**CLOSE**	NO
Ethyl propionate	Ester	KU	NO	NO	NO
Formic acid	Carboxylic Acid	UiO	**YES**	**YES**	**YES**
Formaldehyde	Aldehyde	UiO	**SOME**	**YES**	**YES**
Glyoxal	Aldehyde	Eurochamp	**YES**	**YES**	**YES**
Glyxolylic acid	Acid	Eurochamp	NO	NO	NO
Isopropyl	Alkane	KU	NO	NO	NO
Isopropyl aldehyde	Aldehyde	KU	NO	NO	NO
Methane	Alkane	KU	NO	NO	NO
Metanol	Alcohol	KU	**CLOSE**	**CLOSE**	**CLOSE**
Methyl vinyl ether	Ether	KU	NO	NO	NO
Methyl acetate	Ester	KU	NO	NO	NO
Methyl formate	Ester	NIST	NO	**CLOSE**	NO
Methyl methacrylate	Ester	KU	NO	NO	NO
Propanol	Alcohol	NIST	**CLOSE**	NO	NO
Propioaldehyde	Aldehyde	KU	NO	NO	NO
Propyl acetate	Ester	KU	NO	NO	NO
Propyl formate	Ester	KU	NO	**CLOSE**	NO
THF	Furan	KU	NO	NO	NO

List of Published Master Theses

Department of Physical Geography and Ecosystem Science, Lund University

The student thesis reports are available at the Geo-Library, Department of Physical Geography and Ecosystem Science, University of Lund, Sölvegatan 12, S-223 62 Lund, Sweden. Report series started 1985. The complete list and electronic versions are also electronic available at the LUP student papers (https://lup.lub.lu.se/student-papers/search/) and through the Geo-library (www.geobib.lu.se)

320 Jurgen van Tiggelen (2014) Assimilation of satellite data and in-situ data for the improvement of global radiation maps in the Netherlands.

321 Sam Khallaghi (2014) Posidonia Oceanica habitat mapping in shallow coastal waters along Losinj Island, Croatia using Geoeye-1 multispectral imagery.

322 Patrizia Vollmar (2014) The influence of climate and land cover on wildfire patterns in the conterminous United States

323 Marco Giljum (2014) Object-Based Classification of Vegetation at Stordalen Mire near Abisko by using High-Resolution Aerial Imagery

324 Marit Aalrust Ripel (2014) Natural hazards and farmers experience of climate change on highly populated Mount Elgon, Uganda

325 Benjamin Kayatz (2014) Modelling of nitrous oxide emissions from clover grass ley – wheat crop rotations in central eastern Germany - An application of DNDC

326 Maxime Rwaka (2014) An attempt to investigate the impact of 1994 Tutsi Genocide in Rwanda on Landscape using Remote Sensing and GIS analysis

327 Ruibin Xu (2014) Spatial analysis for the distribution of cells in tissue sections

328 Annabelle Finck (2014) Bird biodiversity in relation to forest composition in Sweden

329 Tetiana Svystun (2015) Modeling the potential impact of climate change on the distribution of Western Corn Rootworm in Europe"

330 Joel Forsmoo (2014) The European Corn Borer in Sweden: A Future Perspective Based on a Phenological Model Approach

331 Andrew Ekoka Mwambo (2015) Estimation of Cropland Ecological Footprint within Danish Climate Commissions 2050 Scenarios for Land use and Bioenergy Consumption

332 Anna Lindstein (2015) Land- atmosphere exchange of carbon dioxide in a high Arctic fen: importance of wintertime fluxes

333 Karla Susana Markley Vergara (2015) Present and near future water availability for closing yield gaps in four crops in South America

334 Klara Århem & Fredrik Fredén (2015) Land cover change and its influence on soil erosion in the Mara region, Tanzania: Using satellite remote sensing and the Revised Universal Soil Loss Equation (RUSLE) to map land degradation between 1986 and 2013

335 Fei Lu (2015) Compute a Crowdedness Index on Historical GIS Data- A Case Study of Hög Parish, Sweden, 1812-1920

336 Lina Allesson (2015) Impact of photo-chemical processing of dissolved organic carbon on the bacterial respiratory quotient in aquatic ecosystems

337 Andreas Kiik (2015) Cartographic design of thematic polygons: a comparison using eye-movement metrics analysis

338 Iain Lednor (2015) Testing the robustness of the Plant Phenology Index to changes in temperature

339 Louise Bradshaw (2015) Submerged Landscapes - Locating Mesolithic settlements in Blekinge, Sweden

340 Elisabeth Maria Farrington (2015) The water crisis in Gaborone: Investigating the underlying factors resulting in the 'failure' of the Gaborone Dam, Botswana

341 Annie Forssblad (2015) Utvärdering av miljöersättning för odlingslandskapets värdefulla träd

342 Iris Behrens, Linn Gardell (2015) Water quality in Apac-, Mbale- & Lira district, Uganda - A field study evaluating problems and suitable solutions

343 Linnéa Larsson (2015) Analys av framtida översvämningsrisker i Malmö - En fallstudie av Castellums fastigheter

344 Ida Pettersson (2015) Comparing Ips Typographus and Dendroctonus ponderosas response to climate change with the use of phenology models

345 Frida Ulfves (2015) Classifying and Localizing Areas of Forest at Risk of Storm Damage in Kronoberg County

346 Alexander Nordström (2015) Förslag på dammar och skyddsområde med hjälp av GIS: En studie om löv- och klockgroda i Ystad kommun, Skåne

347 Samanah Seyedi-Shandiz (2015) Automatic Creation of Schematic Maps - A Case Study of the Railway Network at the Swedish Transport Administration

348 Johanna Andersson (2015) Heat Waves and their Impacts on Outdoor Workers – A Case Study in Northern and Eastern Uganda

349 Jimmie Carpman (2015) Spatially varying parameters in observed new particle formation events

350 Mihaela – Mariana Tudoran (2015) Occurrences of insect outbreaks in Sweden in relation to climatic parameters since 1850

351 Maria Gatzouras (2015) Assessment of trampling impact in Icelandic natural areas in experimental plots with focus on image analysis of digital photographs

352 Gustav Wallner (2015) Estimating and evaluating GPP in the Sahel using MSG/SEVIRI and MODIS satellite data

353 Luisa Teixeira (2015) Exploring the relationships between biodiversity and benthic habitat in the Primeiras and Segundas Protected Area, Mozambique

354 Iris Behrens & Linn Gardell (2015) Water quality in Apac-, Mbale- & Lira district, Uganda - A field study evaluating problems and suitable solutions

355 Viktoria Björklund (2015) Water quality in rivers affected by urbanization: A Case Study in Minas Gerais, Brazil

356 Tara Mellquist (2015) Hållbar dagvattenhantering i Stockholms stad - En riskhanteringsanalys med avseende på långsiktig hållbarhet av Stockholms stads dagvattenhantering i urban miljö

357 Jenny Hansson (2015) Trafikrelaterade luftföroreningar vid förskolor – En studie om kvävedioxidhalter vid förskolor i Malmö

358 Laura Reinelt (2015) Modelling vegetation dynamics and carbon fluxes in a high Arctic mire

359 Emelie Linnéa Graham (2015) Atmospheric reactivity of cyclic ethers of relevance to biofuel combustion

360 Filippo Gualla (2015) Sun position and PV panels: a model to determine the best orientation